RSC Advances

ROYAL SOCIETY OF CHEMISTRY

www.rsc.org/advances

Synthesis and related magnetic properties of $CoFe_2O_4$ cobalt ferrite particles by polyol method with $NaBH_4$ and heat treatment: New micro and nanoscale structures

Nguyen Viet Long [a,b,c,*], Yong Yang [a,*], Toshiharu Teranishi [d], Cao Minh Thi [c], Yanqin Cao [a], Masayuki Nogami [e]

a. State Key Laboratory of High Performance Ceramics and Superfine Microstructure, Shanghai Institute of Ceramics, Chinese Academy of Science, 1295, Dingxi Road, Shanghai 200050, China

b. Posts and Telecommunications Institute of Technology, km 10 Nguyen Trai, Hanoi, Vietnam

c. Ho Chi Minh City University of Technology, 144/24 Dien Bien Phu, Ward-25, Binh Thach, Ho Chi Minh City, Vietnam

d. Faculty of Information, Institute for Chemical Research, Kyoto University, Japan

e. Toyota Physical and Chemical Research Institute, 41-1 Yokomichi Nagakute, 480-1192, Japan

[*]Corresponding author. Email: nguyenviet_long@yahoo.com & yangyong@mail.sic.ac.cn

Shanghai Institute of Ceramics, Chinese Academy of Science, 1295, Dingxi Road, Shanghai 200050, China, Tel:+86-21-52414321; Fax:+86-21-52414219

Abstract. In this contribution, hierarchical $CoFe_2O_4$ particles are successfully prepared via modified polyol elaboration methods with $NaBH_4$ and proposed heat treatment process. Here, new as-prepared $CoFe_2O_4$ particles with a size range of 5μm show high uniform characterization of size, shape and cubic spinel crystal structure by X-ray diffraction (XRD), whole pattern fitting and Rietveld refinement, X-ray photoelectron spectroscopy (XPS), and scanning electron microscopy (SEM). We discover that $CoFe_2O_4$ microparticles prepared in the certain size range of 5μm show exciting configurations of grain and grain boundary under particle heat treatment at high temperature 900°C. Finally, $CoFe_2O_4$ ferrite particles with various well-defined micro and nanoscale structures were produced at appropriate heat treatment processes under high temperature, which has high coercive field, H_C around 416-888 Oe, and the highest saturation magnetization, M_S about 74-91 emu g^{-1} at room temperature (RT) for all the as-prepared samples by vibrating sample magnetometer (VSM). Here, the magnetic behavior has shown persuasive evidences that desirable ferrimagnetic properties of $CoFe_2O_4$ oxides do not only depend on their size but also the spinel structure of $CoFe_2O_4$ oxides as well. Finally, the as-prepared $CoFe_2O_4$ particles with the formula $CoO.Fe_2O_3$ were regarded as the best inverse ferrimagnetic materials with magnetic parameters of H_C at 896 Oe, M_R/M_S squareness around 0.420, M_S around 92 emu g^{-1} at 20 kOe for the downward part of hysteresis loop.

Keywords: Magnetic materials; Ferrite materials; $CoFe_2O_4$; Crystal structure; Heat treatment; clean energy and environment

1. Introduction

At present, magnetic metal- and oxide-based materials have been of importance to convenient, safe, and clean energy-related applications, and key technologies [1-3]. In particular, Fe_2O_3, Fe_3O_4, and general formula of ferrite compounds being $MO{\cdot}Fe_2O_3$ or MFe_2O_4 or $M^{II}Fe^{III}{}_2O_4$ with special micro-, nano-, and nano-to-microscale structures (M = Mn, Co, Ni, Cu or Zn etc.) are ferrite materials with indispensable applications for our health, life, society, clean energy, green science and technology etc in dealing with problems and challenges of serious environmental pollution in 21st century [3-14]. It is known that Fe-, Co-, Ni-based ferrite oxides have inverse spinel structures. In comparison with normal spinel $ZnFe_2O_4$ structure, $CoFe_2O_4$ spinel structures exhibited large positive anisotropy constant. The anisotropy and exchange energy made its magnetic properties between soft and hard ferrite [1a,1c,3a]. Among other transition metal oxides, this material has longitudinal anisotropy in comparison with transverse anisotropy. Here, Curie temperature (Tc) of magnetic materials influenced on the magnetic status of the material. It possibly leads ferrimagnetic properties of $CoFe_2O_4$ materials to be changed into their paramagnetic properties [1-3].

Although various commercial Fe-, Ni-, Co-based ferrite powders were produced in decades ago, they enabled large potential of modern applications and technologies of magnetic recording media, various lithiumion batteries (LIBs) and fuel cells (FCs) for sustainable development of energy and environment [2,3,15,16,27,32,33]. In recent years, Co-, Ni-, and Fe-based ferrites with inexpensive costs have been of commercial importance, such as microwave components and defense applications [1,2,27]. With continuous modifications and improvements of production processes, scientists have facilely prepared $CoFe_2O_4$ or so-called spinel-type $CoFe_2O_4$ materials by hydrothermal processes from various Fe and Co precursors. They could carry out the controlled synthesis of Co-, Ni-, and Fe-based ferrite materials by physical and chemical approach methods. Additionally, researchers obtained Fe_3O_4, $CoFe_2O_4$, $MnFe_2O_4$, etc. or other modern ferrites with various size ranges of 1-100nm, 100-1000nm and 1000-10,000nm (1-10μm) by feasible synthesis

and preparation methods [1-8]. Recently, scholars proved that M_S parameter of $CoFe_2O_4$ ferrite materials are commonly higher than that of other ferrite materials, such as $NiFe_2O_4$, $ZnFe_2O_4$, and $CuFe_2O_4$ etc when the contents of Co or other transitional metal elements in their structures were varied [17-23]. In $CoFe_2O_4$ ferrites, e.g. AB_2O_4 spinel structure, where Fe ions and Co ions refer to tetrahedral and octahedral sites. Therefore, distribution and oxidation states of Co and Fe inside oxide particles need to be clarified.

To address the issues of low cost, high performance, and quality of commercial products in our considerations, $CoFe_2O_4$ particle powders must achieve high homogeneity of size, shape, and structure in a certain range of particle size, which are challenges to scientists. In most cases, $CoFe_2O_4$ particles possess a wide range of particle sizes and shapes. To address other aspects, Ni-, Fe-, Co- and $CoFe_2O_4$-based materials prove interesting properties of coercivity force (H_C), saturation magnetization (M_S), and remanent magnetization (M_r) etc in magnetic hysteresis in respective to the important effects of magnetic domains and walls [1-5,14,27]. Here, most of results of magnetic nanoparticles with critical particle size smaller than 100nm have led to show magnetic property of single magnetic domains under external magnetic field. There is little research that indicated a comparison between two nanosized and microsized ranges of magnetic materials according to magnetism.

In this research, we report the scientific results on the controlled synthesis of high homogeneous $CoFe_2O_4$ particles by modified polyol method with $NaBH_4$ in respective to heat treatment at 900 °C, and show the important evidence of a new structure of $CoFe_2O_4$ particles with grain and grain boundary forms in its high inverse level. Here, the reliable ferrimagnetic properties of $CoFe_2O_4$ ferrite materials with high coercivity and saturation magnetization were discussed in their grain and grain boundary structures of $CoFe_2O_4$ materials as magnetic multidomains. Finally, Fe and Co oxidation states have been found to be 3+ and 2+ inside the best inverse $CoFe_2O_4$ oxides.

2. Experimental section

In controlled synthesis of $CoFe_2O_4$ particles, starting precursors were prepared as described in previous detailed works of α-Fe_2O_3 oxide particles involved [9-12]. Briefly, we paid a lot of attention and time to develop our preparation processes in our best efforts [9-12]. In a typical process, 10mL of EG, 3mL of 0.0625M $FeCl_3$ from $FeCl_3 \cdot 6H_2O$ precursor, 1.5mL of 0.0625M $CoCl_2$ from $CoCl_2 \cdot 6H_2O$ precursor, 10mL of 0.375M PVP, and 0.048g $NaBH_4$ were used for making Sample 1. In the synthesis procedure, the stock solutions of Fe and Co precursors were pumped into reaction flask (250mL), according to a fixed ratio of 2:1 Fe^{3+}/Co^{2+} in volume for exact-controlled synthesis. Similarly, Samples 2 and 3 were prepared with different reaction periods. In processing requirements, reaction periods of Samples 1, 2, and 3 are performed in 25, 35, and 45min, respectively. Then, PVP-CoFe particles were achieved in the resulting black solutions. They were kept at room temperature for some days to obtain black products at the bottom. The clean black products were obtained by removing PVP on the surfaces of as-prepared particles according to centrifugation, washing and cleaning procedures. The dried powders were re-dispersed into ethanol and dried at 60°C. To obtain black-brown oxide products of $CoFe_2O_4$ particles, these black powders were isothermally heated at 900°C for 1h with ceramic containers or Pt containers, and in air. Similarly, we prepared various samples for X-ray diffraction (XRD), scanning electron microscopy (SEM) analysis. Samples 2 and 3 were prepared in different periods but the same annealing stage. The most typical characterizations of $CoFe_2O_4$ particles were investigated by XRD, SEM, and VSM methods. The X-ray diffraction patterns of $CoFe_2O_4$ particles were recorded in a 2θ range of 5-95° by X-ray diffractometer (Rigaku-D/max 2550V, 40kV/40mA, CuKα radiation at 1.54056Å). The whole pattern fitting and Rietveld refinement with phase data involved in CoFe2O4 oxide microparticles were used for the automated refinement setup for precise lattice constant determination, and other parameters. Finally, their features of size, shape, and morphology were investigated by field emission (FE)SEM (Magellan-400, FEI, Eindhoven, Netherlands) with SEM and energy dispersive spectroscopy (EDS) methods, and with electron backscatter diffraction

(EBSD) in SIC-CAS, Shanghai, China. The surface chemical bondings were characterized by X-ray photoelectron spectroscopy (XPS) (Escalab 250, Thermo Scientific, Britain). For the XPS analysis, each sample was pre-etched. Thus, the contents of elements in the cobalt iron ferrite structures were determined. In XPS analysis, we obtained the information of initial surfaces, and that of etched surfaces at 2 kV, 1μA, 1.0mm × 1.0mm for 10s before testing to remove the surface impurities. All the peaks have been adjusted in electric-bearing and taking C285 as the reference. To determine the ferrimagnetic properties of as-prepared $CoFe_2O_4$ mentioned, VSM method was applied for our investigation. We have utilized a vibrating sample magnetometer (VSM), Model EV11 at Institute of Physics (IOP), Academy of Science and Technology (VAST), Ho Chi Minh City, Vietnam, for analyzing magnetic characteristics of $CoFe_2O_4$ material evaluated at room temperature (RT), about 293 K a wide range of applied field from -20 kOe to 20 kOe. Here, EV11-VSM can reach fields up to 31 kOe at a sample space of 5 mm and 27 kOe with the temperature chamber, with Signal noise to be 0.1 μemu, and 0.5 μemu, respectively.

3. Results and Discussion

3.1. Crystal structure

In this research, the crystal structure of all the as-prepared samples of $CoFe_2O_4$ ferrite particles was intensively confirmed by our XRD investigation at room temperature. Fig. 1 shows the most important diffraction peaks of $CoFeO_4$ ferrite particles (Sample 1) locating at (111), (220), (311), (222), (400), (422), (511), (440), (533), (731), and possible (hkl) indices, respectively, which significantly depended on the resolution ability of diffractometers. The corresponding values of 2θ(°) were estimated at 18.471, 30.396, 35.765, 37.422, 43.481, 53.831, 57.491, 63.134, 74.679, 90.547, and more 2θ in a 2θ range of 5-95°, respectively. After pattern indexing, we obtained $CoFe_2O_4$ with cubic spinel structure (Fd3m-277: a = b = c = 8.234 Å), all the parameters were listed in Table 1, which are in agreement with the strongest (311) line of PDF-22-1086 in Inorganics Data Section. It has the corresponding values of 2θ(°) at 18.288, 30.084, 35.437, 37.057, 43.058, 53.445, 56.973, 62.585, 74.009, 89.669, and more 2θ in a 2θ range of 5-95°, respectively. Therefore, the

parameters were in good agreement with the standard pattern for typical $CoFe_2O_4$ ferrite materials. The main diffraction peaks were exactly found in the cubic spinel structure of $CoFe_2O_4$ in its crystal growth. In the XRD powder patterns, $CoFe_2O_4$ microstructures with the crystallographic cF56 and Space Group Fd3m(No.227) show lattice constants (a,b,c) equal to 8.3919Å, 8.3919Å, and 8.3919Å in the standard pattern, and with a ratio of c/a=1 (PDF-22-1086, $CoFe_2O_4$ system) by using Software of Materials Data JADE and MDI Material data for XRD pattern processing. In the reflections from lattice constants, the values of d-I or [d(Å)/I_f(%)] were shown to be 4.7994Å/11.3%, 2.9382Å/29.1%, 2.5085Å/100.0%, 2.4011Å/10.8%, 2.0796Å/24.6%, 1.7016Å/9.70%, 1.6017Å/34.0%, 1.4714Å/43.0%, 1.2700Å/11.6%, and 1.0842Å/12.5% (Fig. 1a) in comparison with 4.847Å/10%, 2.968Å/30%, 2.531Å/100%, 2.424Å/8%, 2.099Å/20%, 1.713Å/10%, 1.615Å/30%, 1.483Å/40%, 1.279Å/9%, and 1.092Å/2%, respectively. The strongest outstanding line was revealed to be from the main reflections of the (311) planes. Therefore, $CoFe_2O_4$ particles show high crystallization of crystal structure of $CoFe_2O_4$ by modified polyol method with $NaBH_4$, and heat treatments at about 900°C to remove all the kinds of PVP polymer remaining and covering on the surfaces, and possibly existing inside of the as-prepared microparticles.

Through the whole pattern fitting (WPF), and with WPF and Rietveld refinement options in Jade 6.5, the WPF of the observed data and Rietveld refinement of $CoFe_2O_4$ crystal structures were performed in Fig. 1(b). In MDI Jade 6.5 version, PSF, Pearson-VII, pseudo-Voigt, and Gaussian were defined. pseudo-Voigt phase was selected for WPF and Rietveld Refinement. The WPF refinement of XRD pattern was used for quantitative analysis, determination of precise lattice constants, and structure modeling by refining atomic parameters [37]. Sample 3 was selected for Rietveld and WPF refinement because of the good shape in its performance. For Sample 3, the results of lattice constants are obtained by WPF and Rietveld and WPF refinement with profile shape function for all the phases, i.e. Pseudo-Voigt, Polynomia, λ = 1.54056 Å (Cu/K-α), which are a, b, and c equal to 8.37529, 8.37529, 8.37529 Å with α, β, and γ equal to the same value 90°, respectively. The value of R_{wp} was 2.16%, which indicated the so-called residual error function in

Jade 6.5, which was minimized by means of the non-linear least-squares iterations. Thus, the lattice constant of $CoFe_2O_4$ particles by Rietveld analysis was smaller than that of cobalt iron oxide in the PDF-22-1086 standard pattern.

In addition, the surface properties of the prepared $CoFe_2O_4$ microparticles were characterized by XPS method for the determination of the existence of elements and their valence in the prepared inverse spinel oxide structure according to the XPS measurements. Figs. 2 from A1 to A4 show the initial surfaces of Sample 1, and Figs. 2 from B1 to B4 show the pre-etched surfaces of Sample 1 by XPS methods.

In Fig. 2, the C1s peaks and regions as charge reference described adventitious hydrocarbons inside the prepared sample (Sample 1). The O1s peaks and regions were commonly available, which originated from the prepared $CoFe_2O_4$ oxides and surrounding environment. The XPS spectra of the primary Fe2p and Co2p core levels of Sample 1 of the prepared $CoFe_2O_4$ oxide microparticles are shown in Fig. 2. The Fe2p spectrum in Fig. 2 (A3, B3, C1, D1) exhibited the two peaks at 711.29 and 724 eV, which are identified as the important surface peak of α-Fe_2O_3 with the presence of Fe^{3+} inside $Co^{(II)}Fe^{(III)}{}_2O_4$ oxide. In addition, there are the two common satellite peaks at 719.72 and 733.90 eV that proved the Fe oxidation states inside the prepared $CoFe_2O_4$ as shown in Fig. 2(A3, C1) [38]. However, the two above satellite peaks on the surfaces of $CoFe_2O_4$ microparticles were reduced by etching process for 10 s. The Co2p spectrum exhibited the two main peaks identified at around 780.76 and 796.43 eV, and with the two satellite peaks identified at around 803.47 and 787.05 eV, respectively. The $Co2p_{1/2}$ and $Co2p_{3/2}$ spectra proved for the Co^{2+} valence states. The two main peaks, and the two satellite peaks led to confirm the presence of Co^{2+} inside $Co^{(II)}Fe^{(III)}{}_2O_4$ oxide (Fig. 2: A4, B4, C2 and D2) for the best inverse spinel structures. In the concerned sample on surface, Sample 1 has the satellite peaks, which have best observed in the XPS spectra. In the prepared $CoO.Fe_2O_3$ oxide with the high inverse spinel structure (Fig. 6b), we suggested that Co and Fe ions occupied Tet- and Oct-cation sites according to the results measured by XPS method.

Thus, cation distribution at Tet- and Oct-sites to Co^{2+} and Fe^{3+} in respect with their oxidation states can lead to change T_C and magnetic moment. The highest level of Co^{2+} contents were integrated into Fe oxide particles for the high inverse $CoFe_2O_4$ structure in Figs. 2. It is possible that there is an existence of very small amount of FeO oxide or Fe oxides in the prepared samples, which will lead to the existence of Fe^{2+}, which cannot be resolved by XRD or XPS and other methods.

3.2. Size and shape

Fig. 3 showed the most typical SEM images of $CoFe_2O_4$ ferrite particles, and their characterizations of size, shape and morphology of $CoFe_2O_4$ ferrite particles were also analyzed. We carried out studying in a similar way in the previous works of Fe_2O_3 [3-6]. Fortunately, all the as-prepared samples of $CoFe_2O_4$ particles proved grain and grain boundary inside the real porous structures after high heat treatment at 900°C in air (Fig. 3), which shows a certain range of particle size about 1-5 μm to Samples. The high homogeneous distributions of size, shape, and morphology of $CoFe_2O_4$ particles were confirmed in final ferrite products. The high rough convex and concave surfaces of grains were observed in their interfaces via grain boundaries. The self-assembly and self-aggregation of the particles were relatively small at microscale level. Thus, their certain sizes were kept during particle heat treatment but heavy particle deformation was found. They only changed the inner structures of theirs under high temperature into various new structures with oxide grains and grain boundaries like famous polygonal ball models, e.g. C60 with atoms in a nanosized range but such one particle itself indicated some of the best advantages of ball models with the most typical grains and grain boundaries in the microsized ranges for design and optimization of nanomaterials in academic and industrial research (Figs. 3d and 3e). This is a hierarchical way of material structure. Fig. 3 also illustrated multidomain structures of $CoFe_2O_4$ microparticles with the spherical shape, and 3.7 μm in size. In such structural and morphological features, grain boundaries exhibited many right and curve forms. In calculation, a particle has about 303±5 $CoFe_2O_4$ oxide grains with various right or curve grain boundaries between the grains on the surface of the half-section surface of spherical particle (Fig. 3), and about 606±10 $CoFe_2O_4$ oxide grains on the whole

surface of spherical particle with three-dimensional (3D) structure, which was discovered [10-12]. There are the two kinds of small and large oxide grains, fine gains with a smaller size range of 100nm, and coarse grains with a larger size range approximately from 100 to 600nm (0.1-0.6μm). Therefore, $CoFe_2O_4$ oxide particles were regarded as hierarchical micro/nanostructured oxide materials. All the as-prepared particles have the microsized range, and every particle has micro/nanoscale structures with grain and grain boundary. A number amount of oxide grains might be formed in their development from hundreds to thousands of grains just inside one $CoFe_2O_4$ particle. In various progresses, these strong evidences of grains and grain boundaries of Fe oxide particles were discovered and high complexity of their surface and structure deformation in Fe_2O_3 oxide particles intensively explained [10-12].

In this context, oxide grains were considered as single crystal structures with very high stability and durability in our successful preparation processes. Therefore, they show the most characteristic spherical- and polyhedral-type shapes, typically such as plates, spheres, polyhedral shapes, hexagonal shapes etc. However, the samples have different shape and morphology but they show the near similar sizes because of different synthetic periods. It is shown that the final formation of grain and grain boundary structures of $CoFe_2O_4$ particles was realized. In the key points, it is suggested that the important effects of particle heat treatment to the formation and grain growth of stable and durable $CoFe_2O_4$ ferrite structure are very necessary to obtain its specific crystal structure. There is no doubt that Pt/$CoFe_2O_4$ particles with grain and grain boundary will become promising magnetic catalytic materials [4,15], and our scientific results have very large impact in practical applications and technologies of FCs, gas sensors, batteries and supercapacitors. In both theory and practice, the main roles of grain and grain boundary textures are best suited for simulation, computer modeling of grain growth, and explanation of magnetic nanostructures with magnetic domains and walls in the standard measurement of magnetic properties [1-3,26]. In the development and formation of micro/nano structures, the grain arrangement and formation of metal, alloy, metal oxide in the large microsized range show the same rules as those of atom arrangement and

formation of metal nanoparticles and multi-metal oxides in the very small nanosized range. However, we suggest that the above mechanisms and rules of arrangement and formation are completely different. These are still important and challenging topics to scientists in different research fields of science materials such as chemical and physical metallurgy.

Figs. 4 and 5 typically show the clear evidences of chemical analysis of $CoFe_2O_4$ oxide particle about 6 μm by SEM and EDS methods associated with Table 2. The results prove that $Co_{1-x}Fe_{2-y}O_4$ structure has the highest inverse level as $CoFe_2O_4$. For elements in one $Co_{1-x}Fe_{2-y}O_4$ particle, we have apparent the Fe/Co ratios of concentration, wt%, and atomic% to be 26.4/12.9, 49/24.51, and 28.49/13.51, respectively, which are 2.046512, 1.999184, and 2.108808, just mainly for the best determination of K-line series, respectively. Therefore, the as-prepared structures were achieved at the best formation of the crystal phase of $CoFe_2O_4$ oxide, i.e. cobalt iron ferrite with spinel structure (PDF-22-1086, $CoFe_2O_4$ system). However, the clear evidence of the high C content was found the samples that were due to the sample preparation processes in solvent as ethanol for the SEM measurements.

3.3. Magnetism and structure

3.3.1. Ferrimagnetism

In our related investigation of the magnetism of $CoFe_2O_4$ material, the most important measurement parameters include M_R, M_S, H_C, H_S, S, and S^* etc., which were calculated, and analyzed in magnetic hysteresis. Figs. 6a and 7 show hysteresis loop taken to saturation, which are two S and S' points in M-H curve. It typically shows remanent magnetization which M measured at H=0, saturation magnetization at maximum M measured in forward and reverse saturations, coercive field strength at which M/H changes sign, squareness parameter (M_R/Ms), maximum energy loss of hysteresis loop, respectively. For the above parameters, hysteresis loop indicated the magnetic parameters of upward part, downward part, and average value, respectively (Fig. 7). It also indicated both ferrimagnetic and ferromagnetic properties. Therefore, $CoFe_2O_4$ particles are so-called soft

magnetic material category. However, there was a clear trend of magnetic properties of $CoFe_2O_4$ ferrite from ferrimagnetism to paramagnetism, then superparamagnetism property. Here, M_R shows to be a high value approximately 39 emu g^{-1} (-39.681, 38.276, and 38.979 emu g^{-1}). Fig. 6a shows M_S on average to be 91 emu g^{-1} to Sample 1 (91.373, -91.577, and 91.475 emu g^{-1}) corresponding to the proposed inverse $CoO.Fe_2O_3$ spinel structure in Fig. 6b, which is one of the highest values that have been known so far for most of various $CoFe_2O_4$ materials in comparison with recent reports [5-9,14]. Here, H_C shows high coercive field strength equal to around 888 Oe (880.60, -895.65, and 888.13 Oe). All the typical parameters of magnetic hysteresis of as-prepared $CoFe_2O_4$ material were listed in Table 3 for Samples 1, 2, and 3. The ferrimagnetism of as-prepared $CoFe_2O_4$ can be explained by molecular field theory between the two sublattices in AB_2O_4 structure with $M=M_A+M_B$ [1]. On the other hand, magnetite Fe_3O_4 materials with inverted spinel structures have Fe^{3+} ions located at A sites (Tetrahedral A sites or *Tet-A*) and Fe^{2+} ions located at B sites (Octahedral B sites or O*ct-B*). We also can express MFe_2O_4 as $Fe_x^{+3}M_{1-x}^{+2}[Fe_{2-x}^{3+}M_x^{+2}]O_4$ in respect with x = 0 (normal spinel), typically for M = Cd and Zn, and x = 1 (inversed spinel) for other metal ions [3a]. It is proved that Fe^{2+} ions can be also replaced with Co^{2+} ions at B sites in model of spinel structure identified [1-3]. The unit cell contains 32 O^{2-} ions, 8 metal ions on *Tet-A* sites, and 16 metal ions on *Oct-B* sites, for a total number of 56 ions [1a]. There are the relative distribution of magnetic Fe ions on *Tet-A* and *Oct-B* sites when the contents of Co ions were integrated into $CoFe_2O_4$. We suggest that the contents of Co and its integration level into Fe oxide matrices change them into $Co_xFe_2O_4$ ($x\leq1$) with a change of Co content, and into $CoFe_2O_4$ materials that leads to change the (super)paramagnetic properties of Fe oxide structure, typically such as Fe_3O_4 structure, into the ferrimagnetic properties of $CoFe_2O_4$ structure. We also think that the higher ability of replacing Fe ion with Co ion located at Tet-A site or Oct-B site can lead to produce the better $CoFe_2O_4$ structure by various experimenters in the highest limit x=1 during the careful preparation process. Inversely, a system of $Fe_{1-x}Co_2O_4$ ($x\leq1$) with a change of Fe content can be prepared by facile preparation processes [25]. In our consideration, we also propose that Co ions have various

ways integrated into spinel structure, and their possible distribution and occupation into both tetrahedral and octahedral sites of spinel structure. So, there are the various possibilities of locations of Co ions located at a spinel structure, which are normal form $A^{tet}B_2{}^{oct}O_4$, inverse form $B^{et}(A,B)^{oct}O_4$, and the random mixed form $(B_ay)^{Tet}(A_{x1}B_{y1})^{oct}O_4$ (xylem=1 or ≤1; $x_1+y_1=2$ or ≤2) with perfect growth and crystallization in well-organized heat treatment or sintering. Additionally, there is also existence of empty sites in the spinel unit cell of $CoFe_2O_4$. This has been possibly a main cause of controversial arising because the resolution of some diffractometer is not sufficient in order to obtain the exact determination of the remaining minor crystal phases and Rietveld analysis. These can lead to the very minor crystal phases of Coo, Co_3O_4 (or $CoCo_2O_4$ spinel structure) or FeO, Fe_2O_3, Fe_3O_4 (or $FeFe_2O_4$ spinel structure) as well as the very minor possible crystal phases of cubic $FeCo_2O_4$ ferrite with spinel structure, and hexagonal ferrites $CoFe_{12}O_{19}$ with magnetoplumbite structure [27] according to preparation and heat treatment processes used. They coexisted in cobalt iron ferrite with the major phase of $CoFe_2O_4$, e.g. AB_2O_4, which resulted in different results of paramagnetic or ferromagnetic or ferrimagnetic properties of hysteresis loops in various works [17-25,27,28]. Thus, extra amount of Co or Fe precursor will lead the mixture of many phases including the minor phase of Co oxides or Fe oxides inside the major phase of $CoFe_2O_4$, i.e. $FeCo_2O_4$. Usually, all the minor phases are ignored because of the difficulty in observation by the resolution of XRD (Fig. 1a). These are the main reasons and the ways that we can develop oxide-based AB_2O_4 ferrites with the best structures, and with new rare earth AB_2O_4 ferrites. In comparison with our results, $CoFe_2O_4$ ferrites are prepared by methods using oxide precursors, which will lead the un-uniform characterization inside their structures. Additionally, there was a possible case that MFe_2O_4 powders in formation can also have a very small amorphous phase in comparison with the major crystal phase [29-35]. However, cation distribution (i.e. Co^{2+} or Ni^{2+}) was also considered corresponding to incomplete inversion in the case of $CoFe_2O_4$ by density functional theory (DFT) [35]. Thus, prepared $CoFe_2O_4$ material exhibited weak ferromagnetism or ferrimagnetism in magnetic multidomain structures. It possibly leads to a wide range of magnetic

properties of between superparamagnetism without magnetic hysteresis, paramagnetism or antiferromagnetism, and ferrimagnetism or ferromagnetism [17-23]. It turned out that this unique ferrimagnetic characterization was due to the existence of various magnetic small and large multidomains from grain and grain boundary configurations of various as-prepared $CoFe_2O_4$ materials in heat treatment process used [10]. At present, this is a concern of researchers in understanding the growth and formation of ferrite materials of grain and grain boundary as well as their magnetic properties according to the phenomena of magnetic domains and walls [1-3].

3.3.2. Magnetic behavior

In the common nature of micromagnetism and nanomagnetism, our results led that good magnetic hysteresis loop is considered as an ideal-form ferrimagnetic hysteresis in symmetry (Fig. 6), indicating a good magnetic ferrite material, whose remanent magnetizations show absolute value of positive magnetization (M_R) as the same as that of negative magnetization ($-M_R$) in near symmetrical hysteresis loop. In the other hand, positive (H_C) and negative ($-H_C$) coercive field strength or coercivity at the two upward part or downward directions of applied field are the near same values according to magnetic hysteresis. However, some researchers illustrated saturation magnetization of MFe_2O_4 nanoparticles in the size ranges of 10 and 20 nm, i.e. $MnFe_2O_4$, Fe_3O_4, $CoFe_2O_4$, Ni Fe_2O_4, $ZnFe_2O_4$ decreased in order, and M_S to be highest at 86 emu g^{-1} for $MnFe_2O_4$ (16 nm). They are some special cases of superparamagnetic Fe oxide (SPIO) particles [24], and most of MFe_2O_4 materials possibly showed high superparamagnetic properties. Although Sample 1 has M_S and H_C showing the highest saturation magnetization and coercive field in Fig. 7. However, our prepared samples have shown good ferrimagnetic properties of $CoFe_2O_4$ particle powders in a microsized range (5μm) in comparison with superparamagnetic properties of MFe_2O_4 particles of a nanosized range (20nm) (M=Mn, Fe, Co, and Ni) [24], typically such as M_S=86 emu g^{-1} for $MnFe_2O_4$ nanoparticles with 16 nm in size [24] as well as MFe_2O_4 (M=Mn^{2+}, Fe^{2+}, Co^{2+}, Ni^{2+}) ferrite spinel [29]. Figs. 6 and 7 evidently illustrated the narrow hysteresis M-H loops, which enable

their large potential applications in high frequency devices [1-3,27]. However, the M_S values of $MnFe_2O_4$ (around 7 nm), $CoFe_2O_4$ (9 nm), $NiFe_2O_4$ (11 nm), and $FeFe_2O_4$ (24 nm) are 23.9, 69.7, 34.2, and 58.6 emu g^{-1}, respectively while their corresponding theoretical values are 120.8, 71.2, 47.5, and 96.2 emu g^{-1}. For structure considerations, the saturation magnetization M_S of $CoFe_2O_4$ particles in the range of 5 μm with grain and grain boundary shows much higher than that of $CoFe_2O_4$ nanoparticles in the size ranges of 25-60 nm and 60-135 nm [24]. In this comparison, these results show a difference between the nanosized and microsized ranges of $CoFe_2O_4$, and between their micro and nanostructures. The behavior of micromagnetism and nanomagnetism of Fe-based oxides are relatively similar in the magnetic hysteresis loops [34]. This can be possibly true among soft and hard ferrimagnetic materials with many categories of their bulk, film, and particle powder in their modifications. Fig. 8 illustrated hierarchical magnetic oxide particles with oxide grains and grain boundaries corresponding to the obtained results in our research. Therefore, their shapes and morphologies can be controlled in various polyhedral and spherical forms. Overall, we reconfirmed that the prime importance and the effects of shape and structure of magnetic alloys and ferrites are also the same as that of the size in miro/nanoscale materials while they have a huge potential of commercial, industrial, academic, military, and space applications [27,36].

4. Conclusion

In this research, the hierarchical $CoFe_2O_4$ ferrite microparticles were made by the two constituent mixtures of $FeCl_3$ and $CoCl_2$ precursors. Here, we aimed to study synthesis and preparation processes of $CoFe_2O_4$ particle powders with high homogeneous distribution of particle size and crystalline structure in the as-prepared oxide products. We have tried to achieve the most successful preparation of $CoFe_2O_4$ particle powders in efforts of process optimization with preparation and experimental conditions. They possess specific grain and grain boundary microstructure, and with regard to high crystallization of ferrimagnetism. It is predicted that the high density of the grains and boundaries inside the prepared oxide microparticles that can lead high ferrimagnetic property of $CoFe_2O_4$ microparticles with the main valence states occupied to be +2 for Co, and +3 for Fe. We

have presented a new approach to preparation process of grain and grain boundary textures of new $CoFe_2O_4$ ferrites, and obtained the best ferrimagnetic properties of $CoFe_2O_4$ ferrite materials in the range of 5μm in size. We suggested that there are the various spinel structures that are $Co^{tet}Fe_2{}^{oct}O_4$, $Fe^{tet}(Fe,Co)^{oct}O_4$, and $(Co_xFe_y)^{tet}(Fe_{x1}Co_{y1})^{oct}O_4$ (x+y=1, and $x_1+y_1=2$). Here, A and B indicated Fe and Co ions. Therefore, Co cation distribution in cobalt iron ferrites reached the highest degree, which is in the level of the best inversion when x=o and y=o according to the much simpler formula of $Co_{1-x}Fe_{2-y}O_4$ spinel structure. Our preparation process shows high stability and repetition of $CoFe_2O_4$ products. Finally, not only crystal features of $CoFe_2O_4$ particles are clarified but also importance of ferrimagnetic properties is discussed to micro/nanoscale structures.

Acknowledgment

We are grateful to precious support through Visiting Fellowship for Researchers from Developing Countries (Grant No. 2013FFGB0007) and China Postdoctoral Science Foundation (No. 2014M551462) in the period of 2013-2015 from Shanghai Institute of Ceramics, Chinese Academy of Science, Dingxi Road 1295, Shanghai 200050, China.

Conflict of interest

The authors declare no conflict of interest.

References

1. (a) S. Chikazumi, Physics of Ferromagnetism (International Series of Monographs on Physics), Edition 2nd, Published in the United States, Oxford University Press Inc., New York, 2009. (b) A. Goldman, *Modern ferrite technology*, 2nd edition, Springer, Science-Business Media, Inc., 2006.
2. R. M. Cornell, U. Schwertmann, *The Iron Oxides: Structure, Properties, Reactions, Occourences and Uses*, John Wiley & Sons, Inc., Verlag GmbH&Co. KGaA, Weinheim, 2003.
3. (a) K. H. J Buschow, F. R. de Boer, *Physics of Magnetism and Magnetic Materials*, Springer, 2003. (b) J. M. D. Coey, *Magnetism and Magnetic Materials*, Cambrige Press, 2010. (c) T. Miyazaki, H. Jin, *The Physics of Ferromagnetism*, Vol. 158, Springer Series in Materials,

Science Springer, Verlag, Berlin, Heidelberg 2012. (d) Y. Liu, D. J. Sellmyer, D. Shindo, *Handbook of Advanced Magnetic Materials,* Springer Science, Business Media, Inc. 2006.

4. C. Yuan, H. B. Wu, Y. Xie, X. W. Lou, Angew. Chem. Int. Ed., 2014, **53**, 1488-1504.
5. M. Abbas, M. N. Islam, B. P. Rao, K. E. A. Aitah, C. Kim, Mater. Lett., 2015, **139**, 161-164.
6. L. Lv, Q. Xu, R. Ding, L. Qi, W. Wang, Mater. Lett., 2013, **111**, 35-38.
7. N. Dong, F. He, J. Xin, Q. Wang, Z. Lei, S. Su, Mater. Lett., 2015, **141**, 238-241.
8. L. Khalil, C. Eid, M. Bechelany, N. Abboud, A. Khoury, P. Miele, Mater. Lett., 2015, **140,** 27-30.
9. D. Zhang, X. Zhang, X. Ni, J. Song, H. Zheng, J. Magn. Magn. Mater., 2006, **305**, 68-70.
10. N. V. Long, Y. Yang, C. M. Thi, Y. Cao, M. Nogami, Colloids Surf. A, 2014, **456**, 184-194.
11. N. V. Long, Y. Yang, M. Yuasa, C. M. Thi, Y. Cao, T. Nann, M. Nogami, RSC. Adv., 2014, **4**, 8250-8255.
12. N. V. Long, Y. Yang, M. Yuasa, C. M. Thi, Y. Cao, T. Nann, M. Nogami, RSC. Adv., 2014, **4**, 6383-6390.
13. N. V. Long, Y. Yang, B. T. Hang, Y. Cao, C. M. Thi, M. Nogami, Colloid Polym. Sci., 2015, **293**, 49-63.
14. R. Iano, Mater. Lett., 2014, **135**, 24-26.
15. N. V. Long, Y. Yang, C. M. Thi, Y. Cao, N. V. Minh, M. Nogami, Nano Energy, 2013, **2**, 636-676-676.
16. A.R. Jha, *Rare Earth Materials Properties and Applications*, CRC Press, Taylor & Francis Group 6000 Broken Sound Parkway NW, Suite 300, Boca Raton, FL33487-2742, 2014.
17. M. Dong, Q. Lin, D. Chen, X. Fu, M. Wang, Q. Wu, X. Chen, S. Li, RSC Adv., 2013, **3**, 11628-11633.
18. R. Sharma, S. Bansal, and S. Singhal, RSC Adv., 2015, **5**, 6006-6018.
19. Z. Zhang, W. Ren, Y. Wang, J. Yang, Q. Tan, Z. Zhong, and F. Su, Nanoscale, 2014, **6**, 6805-6811.
20. H. Guo, T. Li, W. Chen, L. Liu, X. Yang, Y. Wang, and Y. Guo, Nanoscale, 2014, **6**, 15168-15174.
21. W. Yang, Y. Yu, L. Wang, C. Yang, and H. Li, Nanoscale, 2015, **7**, 2877- 2882.
22. D. Primc, and D. Makovec, Nanoscale, 2015, **7**, 2688-2697.
23. N. Lee, T. Hyeon, Chem. Soc. Rev., 2012, **41**, 2575-2589.
24. (a) J. Mohapatra, A. Mitra, D. Bahadur, M. Aslam, CrystEngComm., 2013, **15**, 524-532. (b) J. Mohapatra, S. Nigam, J. Gupta, A. Mitra, M. Aslam, D. Bahadur, RSC Adv., 2015, **5**, 14311-14321.

25. L. Ajroudi, N. Mliki, L. Bessais, V. Madigou, S. Villain, Ch. Leroux, Mater. Res. Bull., 2014, **59**, 49-58.
26. F. Zasada, J. J. Gryboś, P. Indyka, W. Piskorz, J. Kaczmarczyk, and Z. Sojka, J. Phys. Chem. C, 2014, **118**, 19085-19097.
27. R. C. Pullar, Prog. Mater Sci., 2012, **57**, 1191-1334.
28. L. Ajroudi, N. Mliki, L. Bessais, V. Madigou, S. Villain, Ch. Leroux, Mater. Res. Bull., 2014, **59**, 49-58.
29. R. Pązik, E. Piasecka, M. Małecka, V. G. Kessler, B. Idzikowski, Z. Śniadecki, R. J. Wiglusz, RSC Adv., 2013, **3**, 12230-12243.
30. K. V. P. M Shafi, A. Ulman, X. Yan, N. Yang, C. Estournes, H. White, M. Rafailovich, Langmuir, 2001, **17**, 5093-5097.
31. N. Bao, L. Shen, Y. Wang, P. Padhan, A. Gupta, J. Am. Chem. Soc., 2007, **129**, 12374- 12375.
32. X. Wu, Z. Lu, W. Zhu, Q. Yang, G. Zhang, J. Liu, X. Sun, Nano Energy, 2014, **10**, 229-234.
33. Y. Xiao, J. Zai, X. Li, Y. Gong, B. Li, Q. Han, X. Qian, Nano Energy, 2014, **6**, 51-58.
34. H. Zeng, J. Li, Z. L. Wang, J. P. Liu, S. Sun, Nano Lett., 2004, **4**, 187-190.
35. D. Fritsch, H. H. Wills, C. Ederer, Phys. Rev. B, 2012, **86**, 014406.
36. V. G. Harris, Microwave Magnetic Materials, in Vol. 20, Handbook of Magnetic Materials, Edited by K. H. J. Buschow, 2012, 1-63.
37. G. Will, Powder Diffraction, *The Rietveld Method and the Two Stage Method to Determine and Refine Crystal Structures from Powder Diffraction Data*, Springer-Verlag Berlin Heidelberg, 2006.
38. K. Zhang , W. Zuo, Z. Wang , J. Liu, T. Li, B. Wang, Z. Yang, RSC Adv, 2015, **5**, 10632-10640.

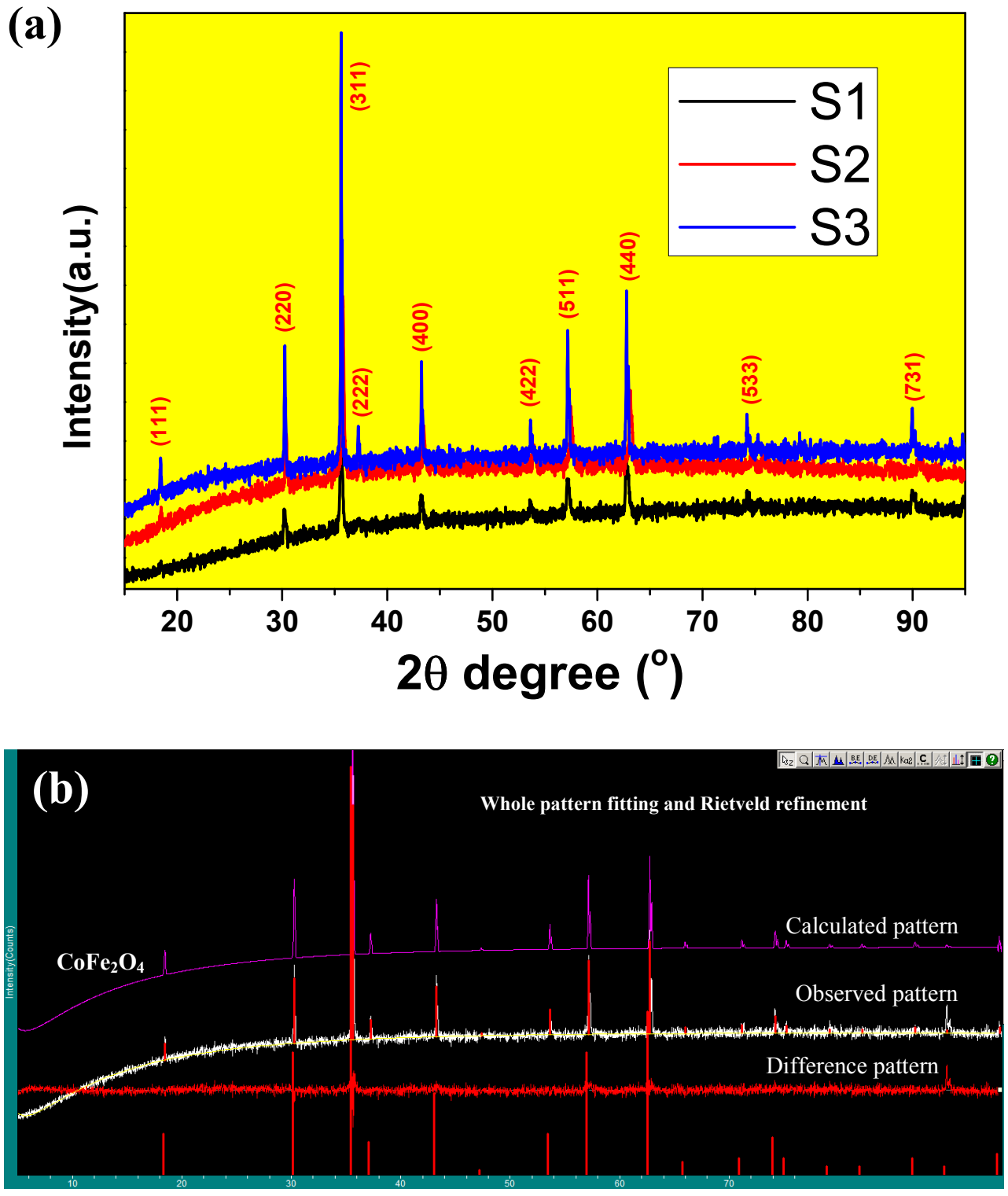

Figure 1. (a) XRD patterns of $CoFe_2O_4$ particles. (b) The whole pattern fitting and Rietveld refinement of $CoFe_2O_4$ oxide microparticles. (a) Calculated pattern; (b) Observed pattern; (d) Difference between Calculated pattern and Observed pattern.

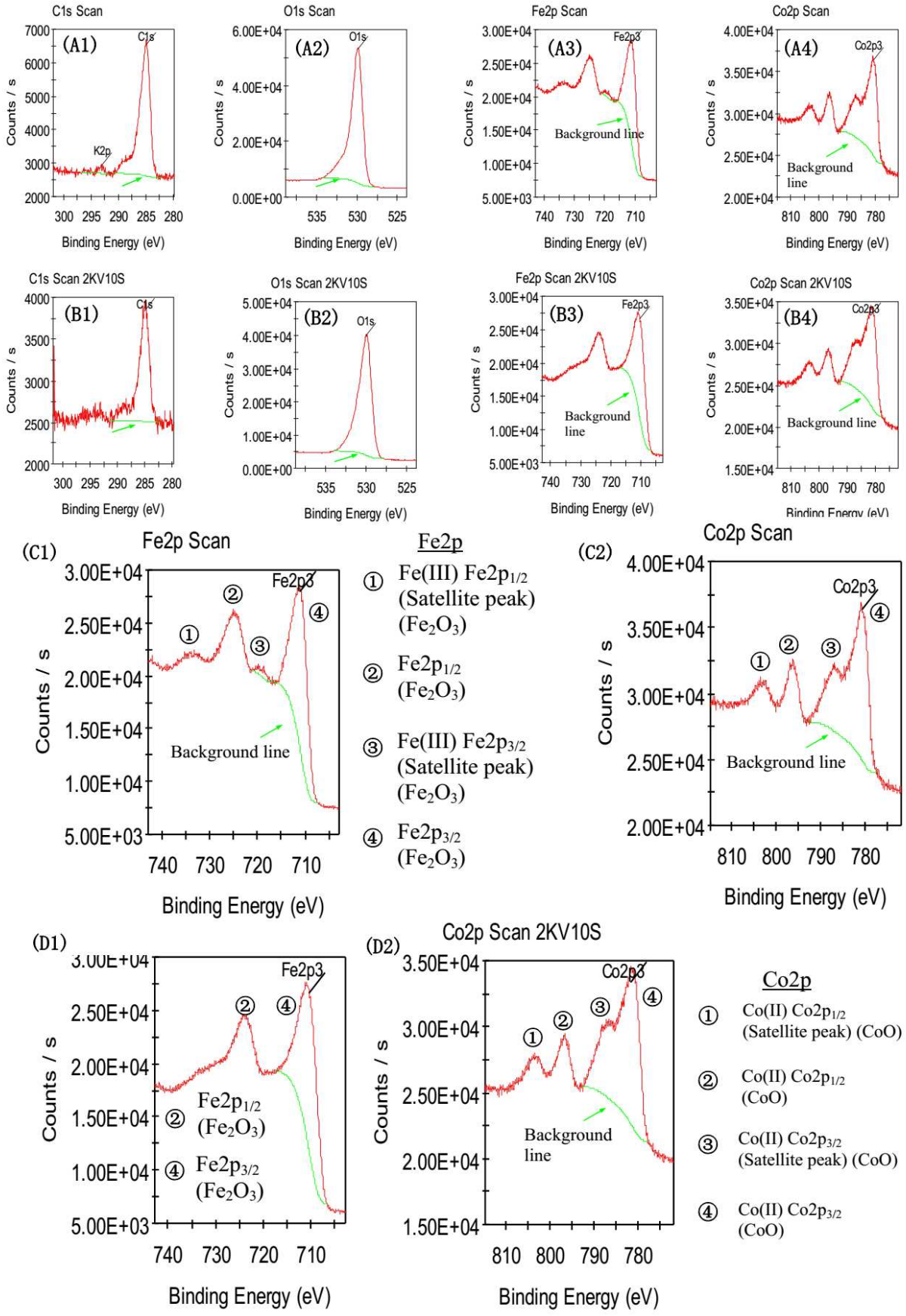

Figure 2. A1-A4: XPS spectra of $CoFe_2O_4$ microparticles with the initial surfaces (Sample 1). B1-B4: XPS spectra of $CoFe_2O_4$ microparticles with the etched surfaces (Sample 1). C1, C2, D1, D2: Comparison of initial surfaces and etched surfaces of $CoFe_2O_4$ microparticles by XPS corresponding to Fe and Co oxidation states inside $CoFe_2O_4$ oxide. Green lines indicate background line of XPS measurements.

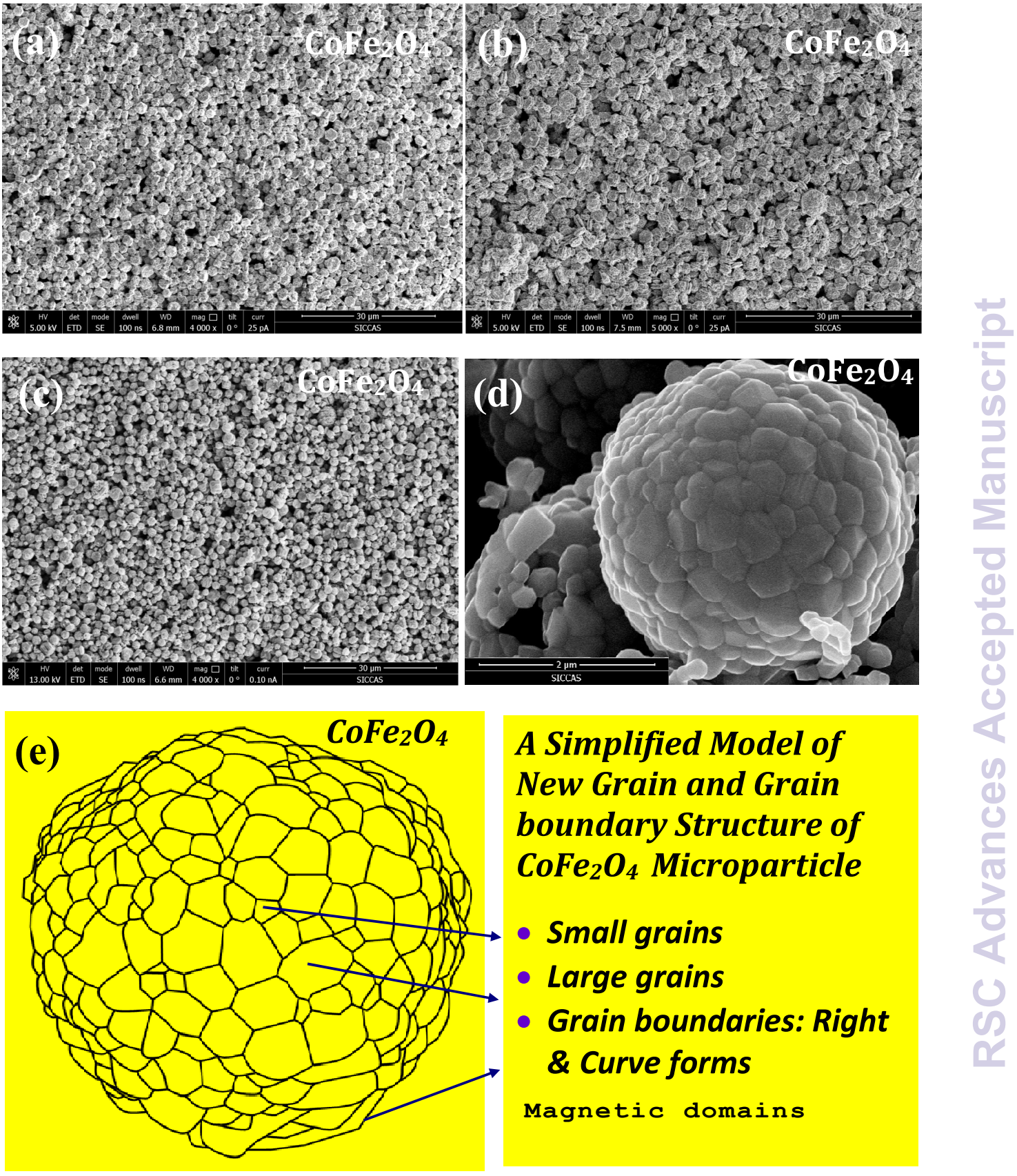

Figure 3. SEM images of $CoFe_2O_4$ particles (a-d). (e) Structural model of $CoFe_2O_4$ microparticles with grain and grain boundary as well as grain arrangement in a spherical model with 606 grains in our results. Scale bars: (a)-(c) 30μm. (d) 2μm.

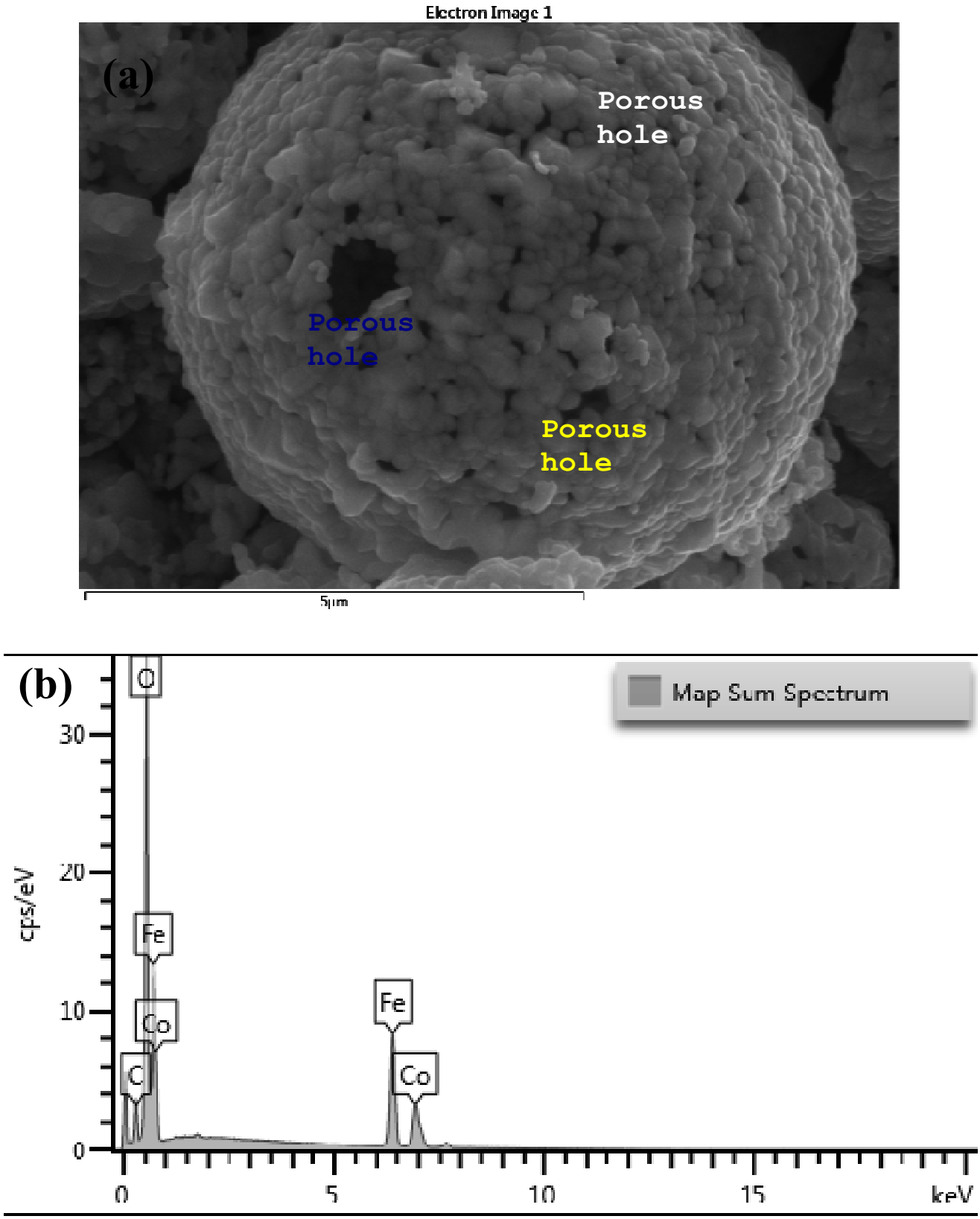

Figure 4. (a) SEM image of $CoFe_2O_4$ oxide particle with a lot of small and large grain and boundary. (b) Existence of elements of one $CoFe_2O_4$ oxide particle by SEM-EDS methods.

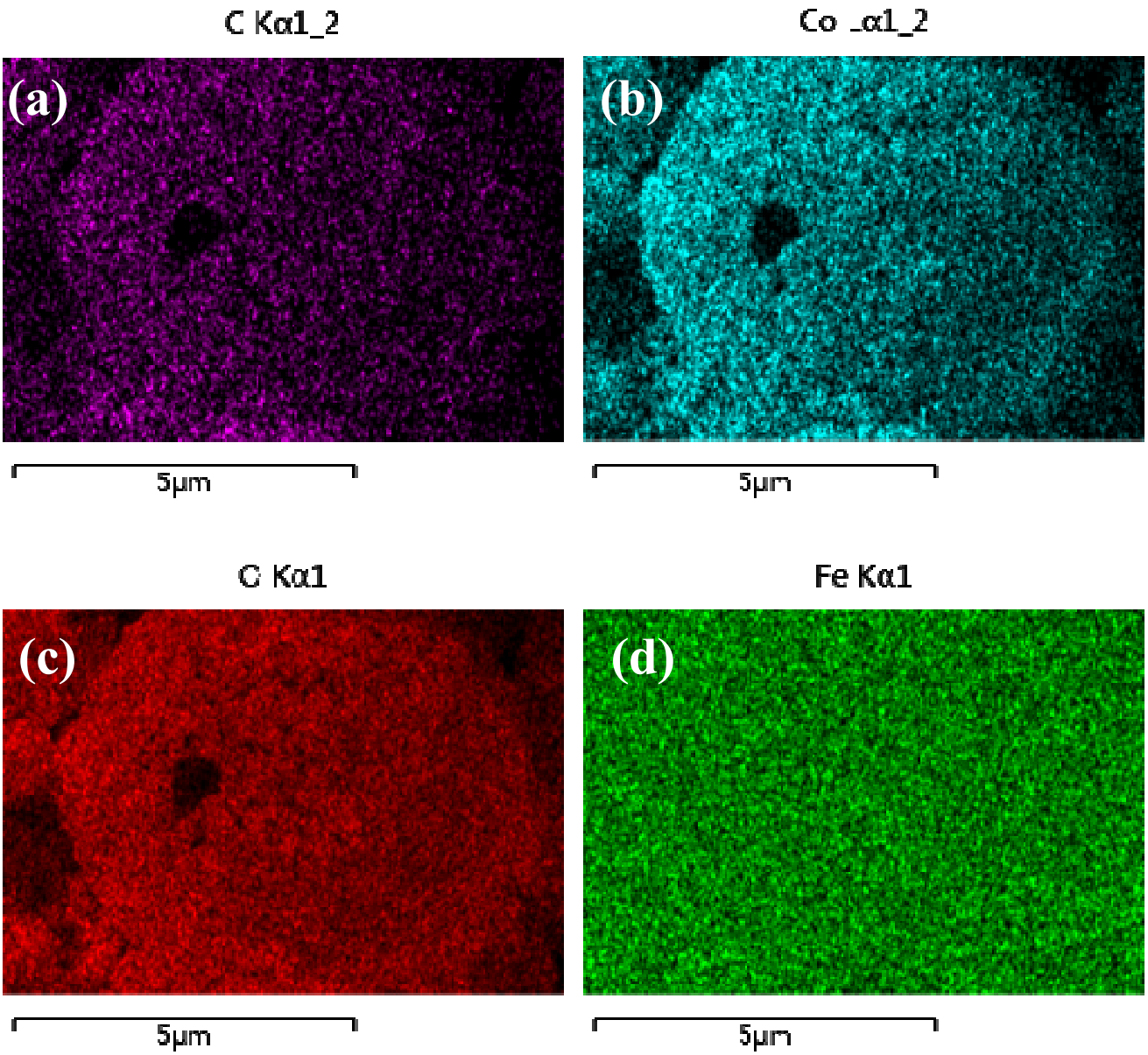

Figure 5. Chemical analysis of $CoFe_2O_4$ oxide particle in the size range of 6 µm associated with EDS and SEM image of $CoFe_2O_4$ particle; (a) C Kα1,2; (b) Co Lα1-2; (c) O Kα1; (d) Fe Kα1. Scale bars: (a-d) 5 µm

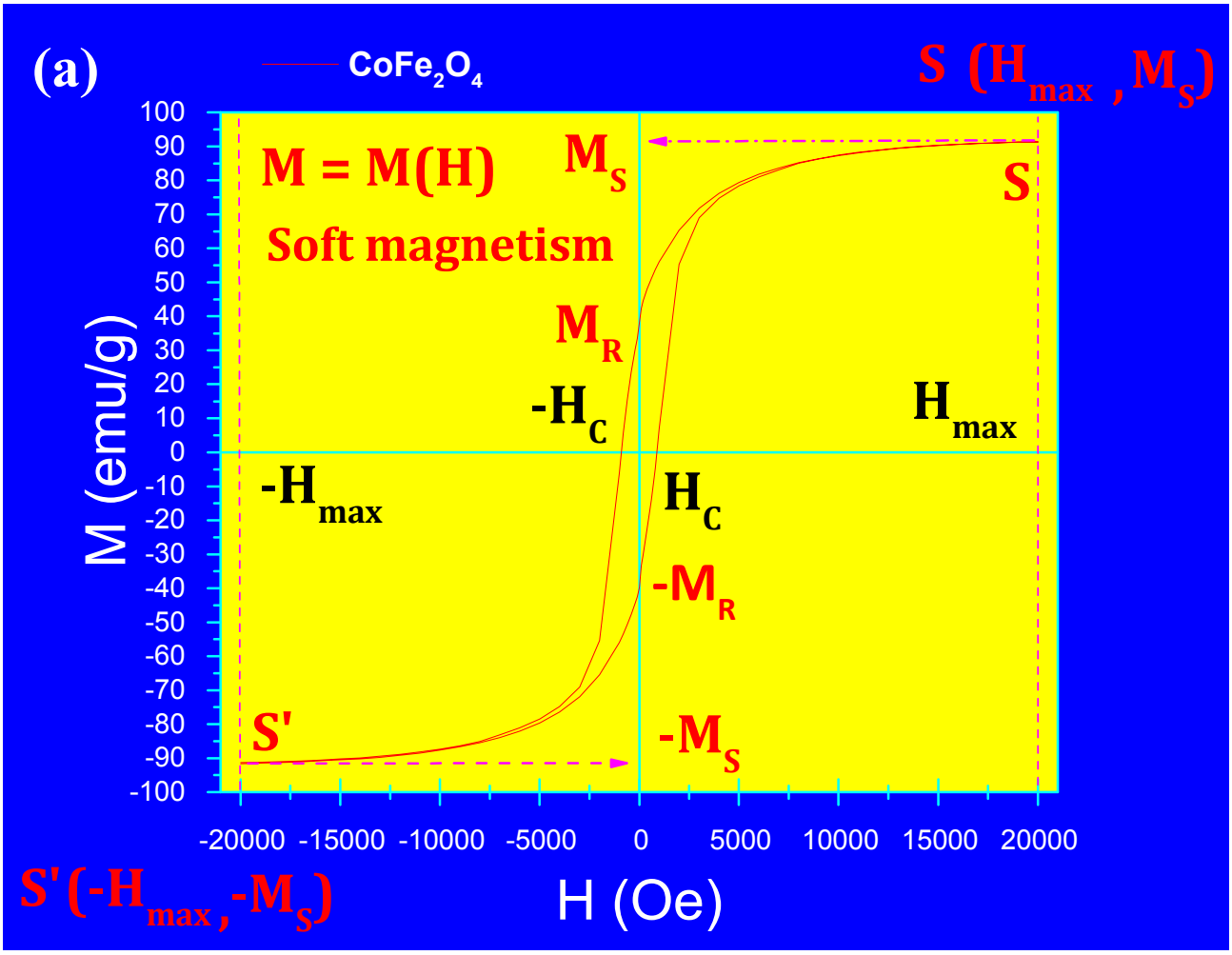

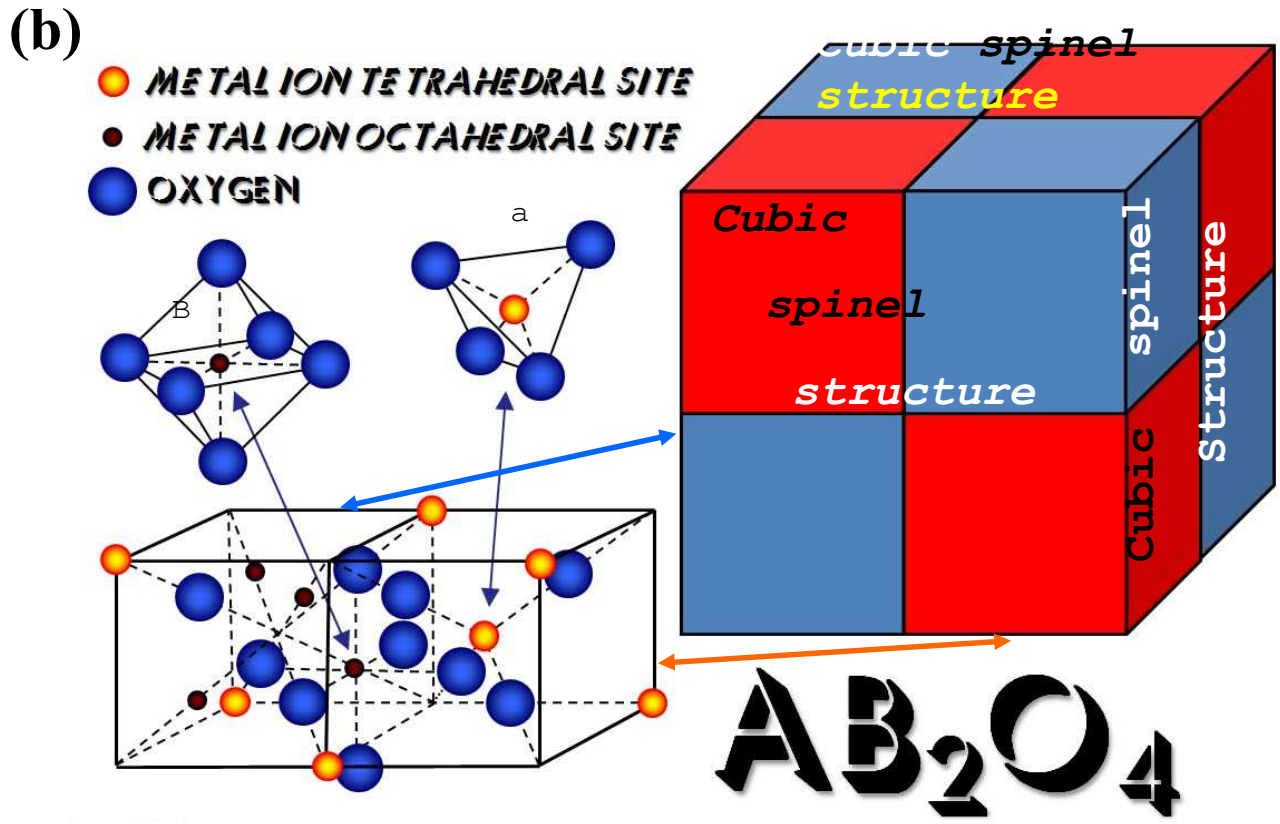

Figure 6. (a) Magnetic hysteresis of $CoFe_2O_4$ (Sample 1). (b) Model of spinel structure of $CoFe_2O_4$

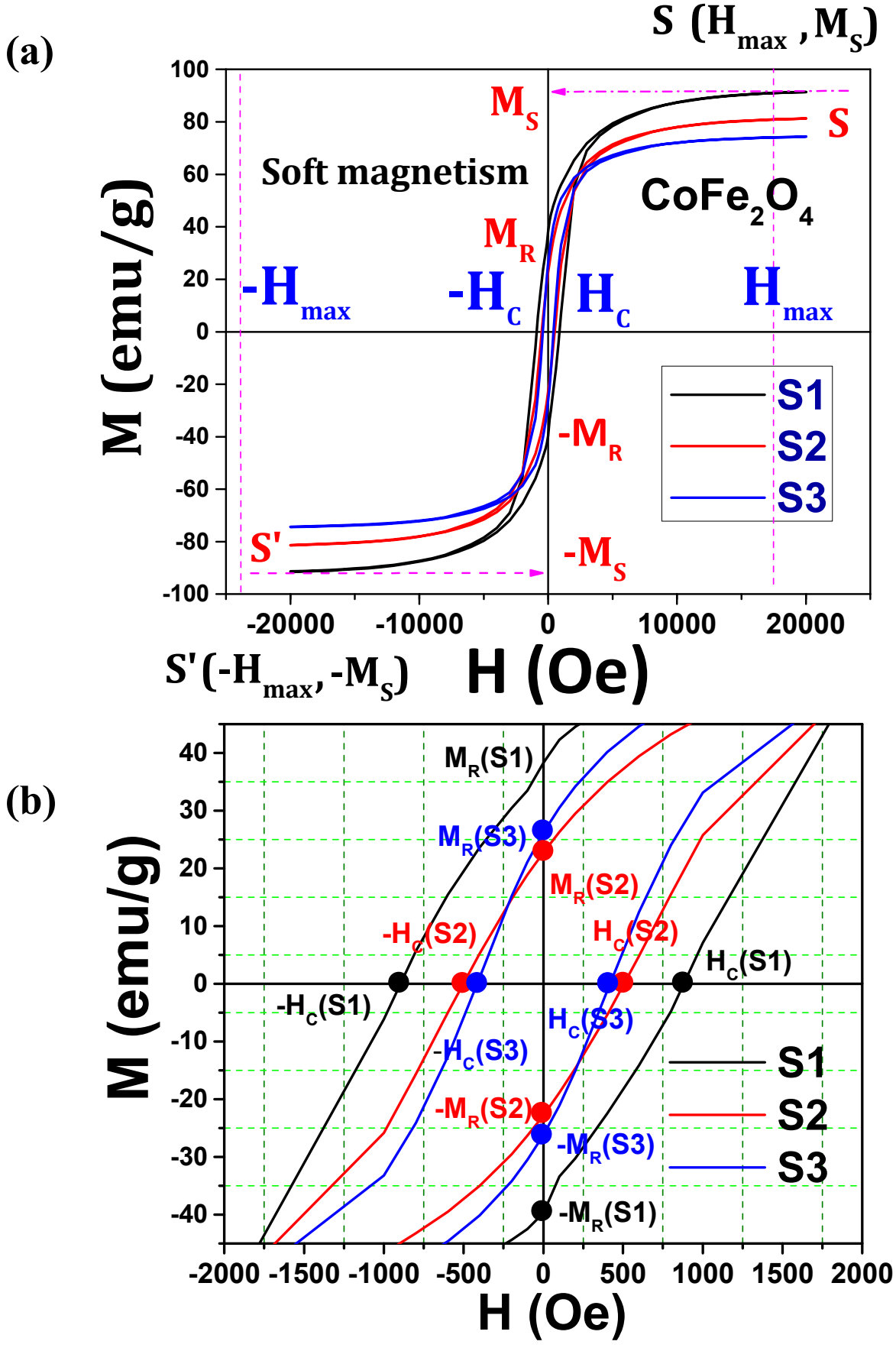

Figure 7. (a) Magnetic hysteresis of $CoFe_2O_4$ (Samples 1,2, and 3). (b) Snapshot of (a).

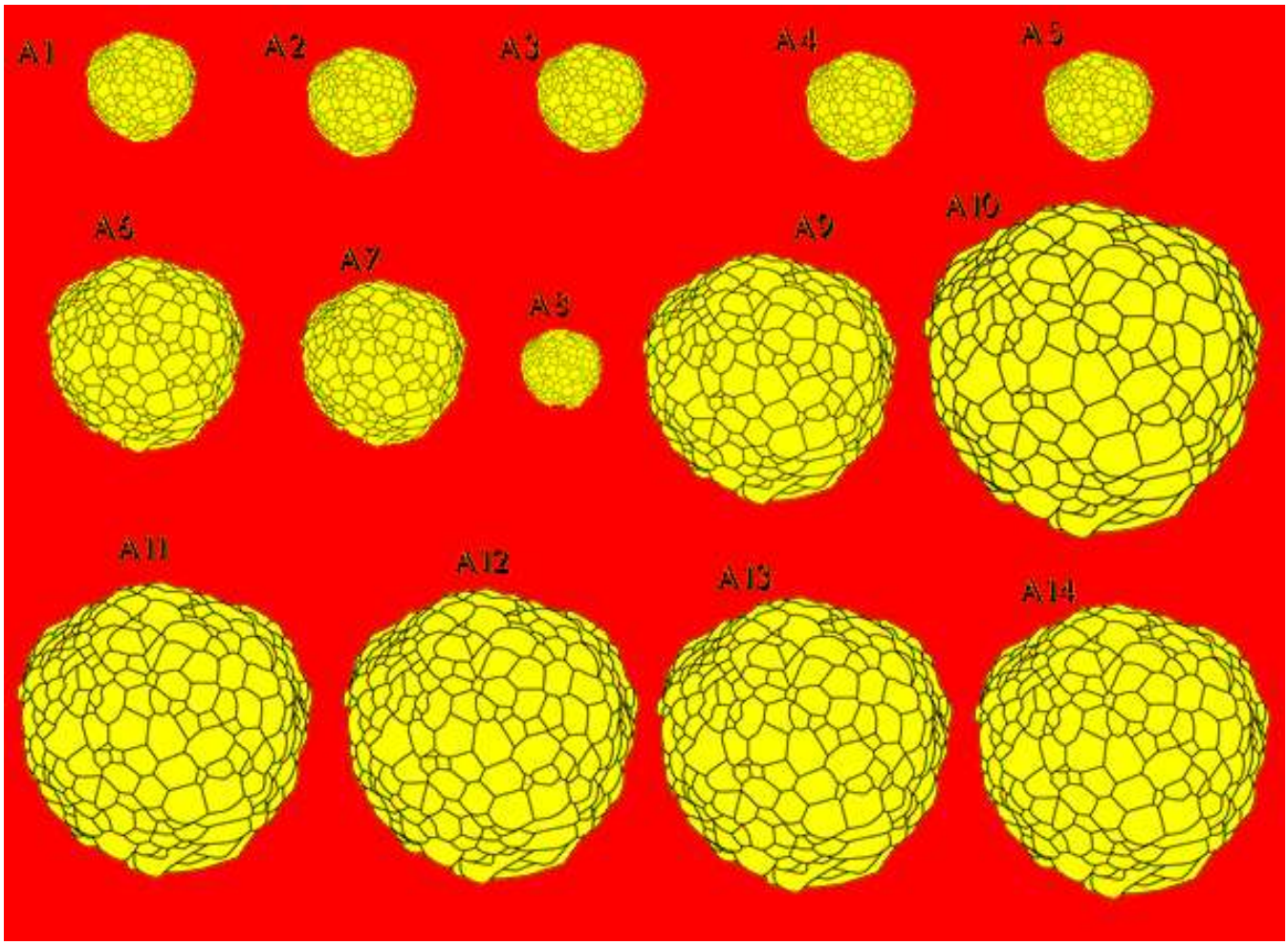

Figure 8. Models of hierarchical particles with grain and grain boundaries (A1-A14).

Table 1. Indexing of $CoFe_2O_4$ with cubic spinel structure (Fd3m-277: a=b=c= 8.234 Å; α=β=γ=90°)			
2Theta (°)	(h k l)	d (Å)	I (%)
18.471	(1 1 1)	4.7994	11.3
30.396	(2 2 0)	2.9382	29.1
35.765	(3 1 1)	2.5085	100.0
37.422	(2 2 2)	2.4011	10.8
43.481	(4 0 0)	2.0796	24.6
53.831	(4 2 2)	1.7016	9.70
57.491	(5 1 1)	1.6017	34.0
63.134	(4 4 0)	1.4714	43.0
74.679	(5 3 3)	1.2700	11.6
90.547	(7 3 1)	1.0842	12.5

Table 2. Chemical analysis of $CoFe_2O_4$ ferrite by SEM-EDS method						
Element	Line Type	Apparent Concentration	k Ratio	Wt% Sigma	Wt%	Atomic %
C	K series	1.15	0.0115	0.11	6.27	16.96
O	K series	23.63	0.07952	0.1	20.22	41.04
Fe	K series	26.4	0.26404	0.19	49	28.49
Co	K series	12.9	0.12899	0.2	24.51	13.51
Total:					100	100

Table 3. Typical magnetic parameters of hysteresis loop by VSM method for the as-prepared weak ferromagnetic or ferrimagnetic $CoFe_2O_4$ materials. Symbols: M_R: Remanent magnetization, M_S: Saturation magnetization, H_C: Coercive field, S: Squareness (M_R/M_S), S': 1-(M_R/H_C)(1/slope at H_C)

Samples	Parameters	Unit	Upward	Downward	Average
Sample 1	M_R	emu g^{-1}	-39.681	38.276	38.979
	M_S	emu g^{-1}	91.373	-91.577	91.475
	H_C	Oe	880.60	-895.65	888.130
	S (M_R/M_S)	Constant	0.430	0.420	0.430
	S*	Constant	0.251	0.246	0.248
Sample 2	M_R	emu g^{-1}	-22.797	22.781	22.789
	M_S	emu g^{-1}	81.331	-81.412	81.372
	H_C	Oe	505.84	-502.25	504.05
	S (M_R/M_S)	Constant	0.280	0.280	0.280
	S*	Constant	0.118	0.111	0.115
Sample 3	M_R	emu g^{-1}	-26.205	26.211	26.208
	M_S	emu g^{-1}	74.375	-74.502	74.439
	H_C	Oe	417.87	-415.08	416.48
	S (M_R/M_S)	Constant	0.350	0.350	0.350
	S*	Constant	0.088	0.088	0.088

Figure 1

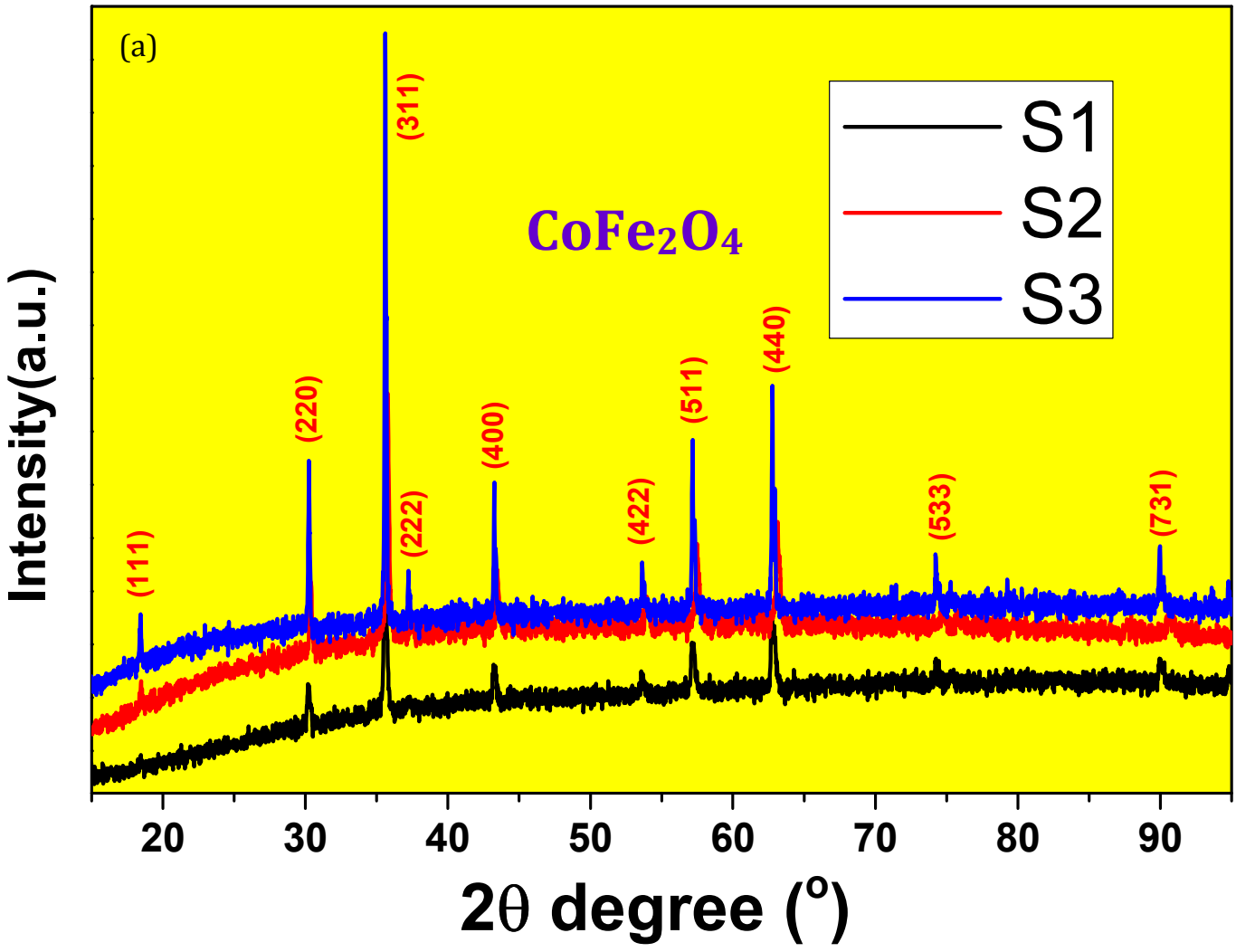

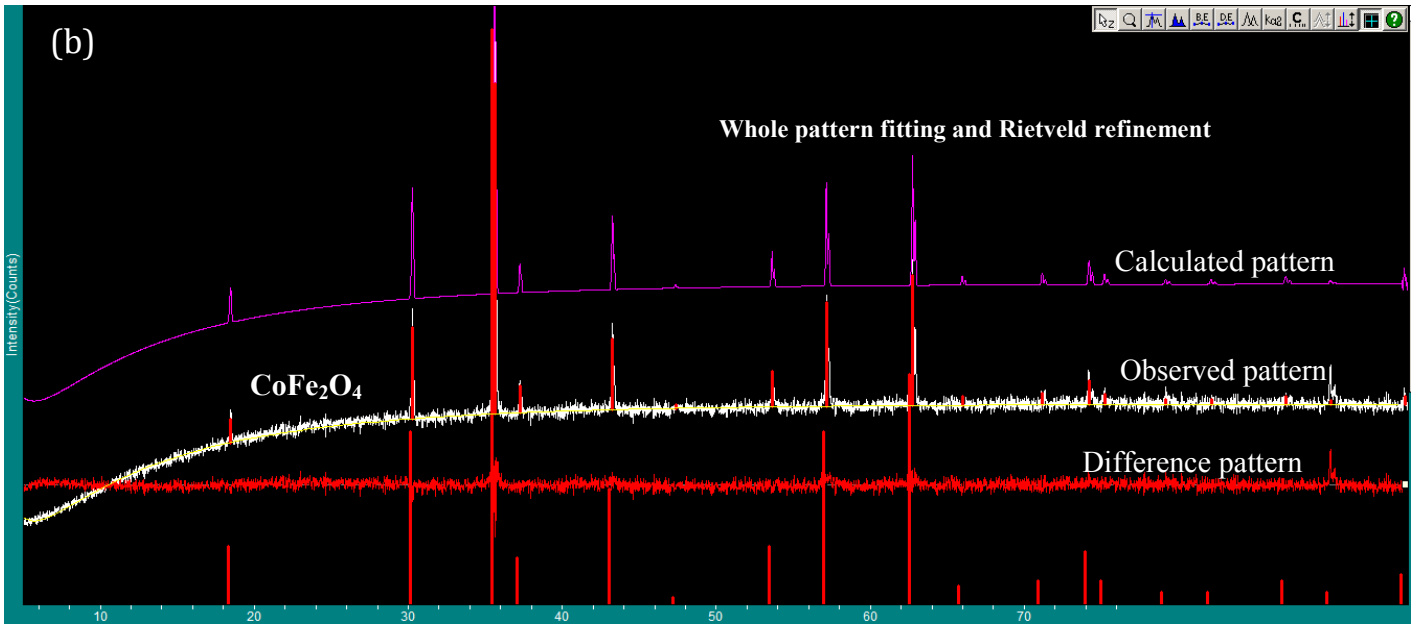

Figure 2

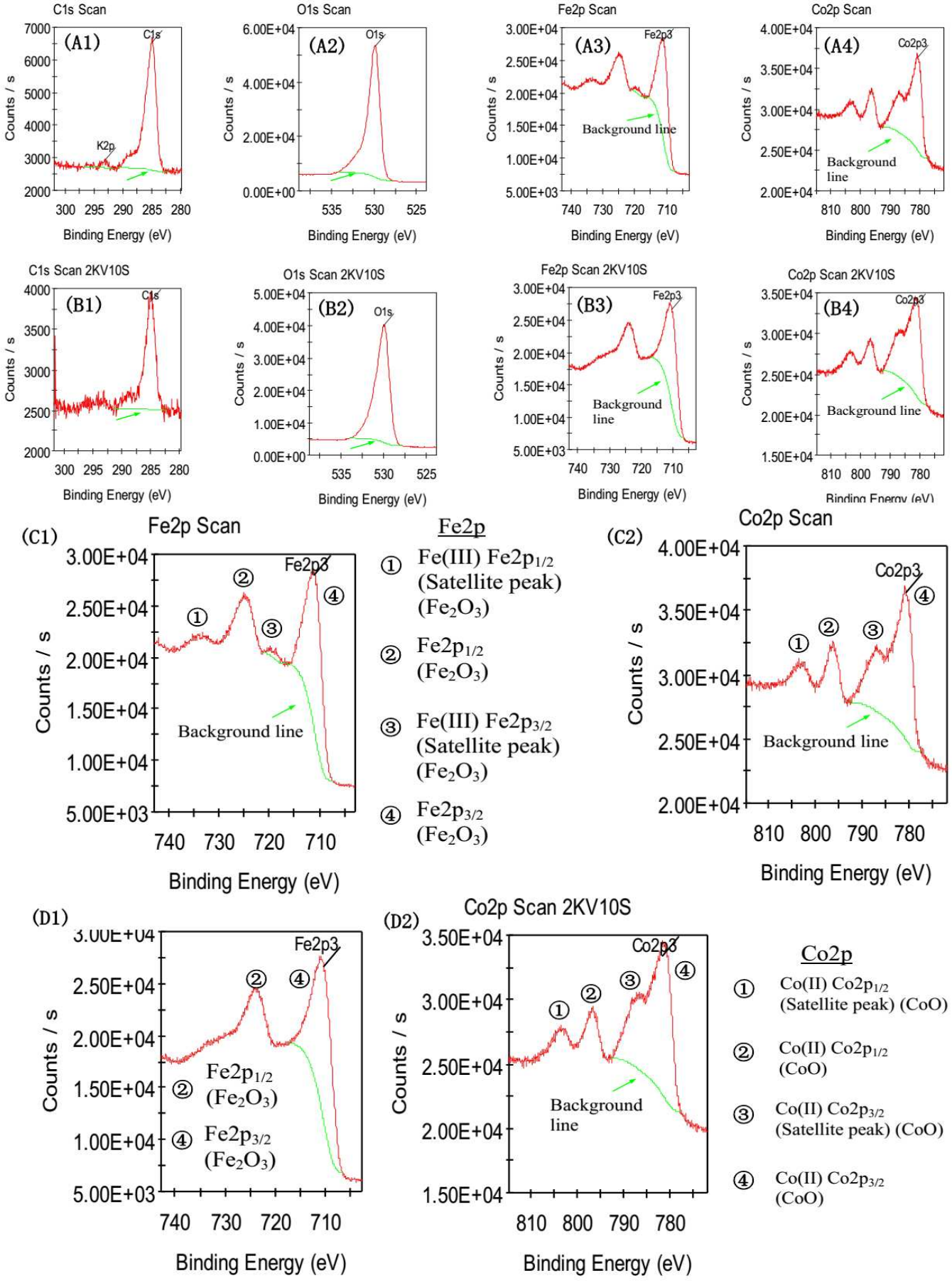

Figure 3a

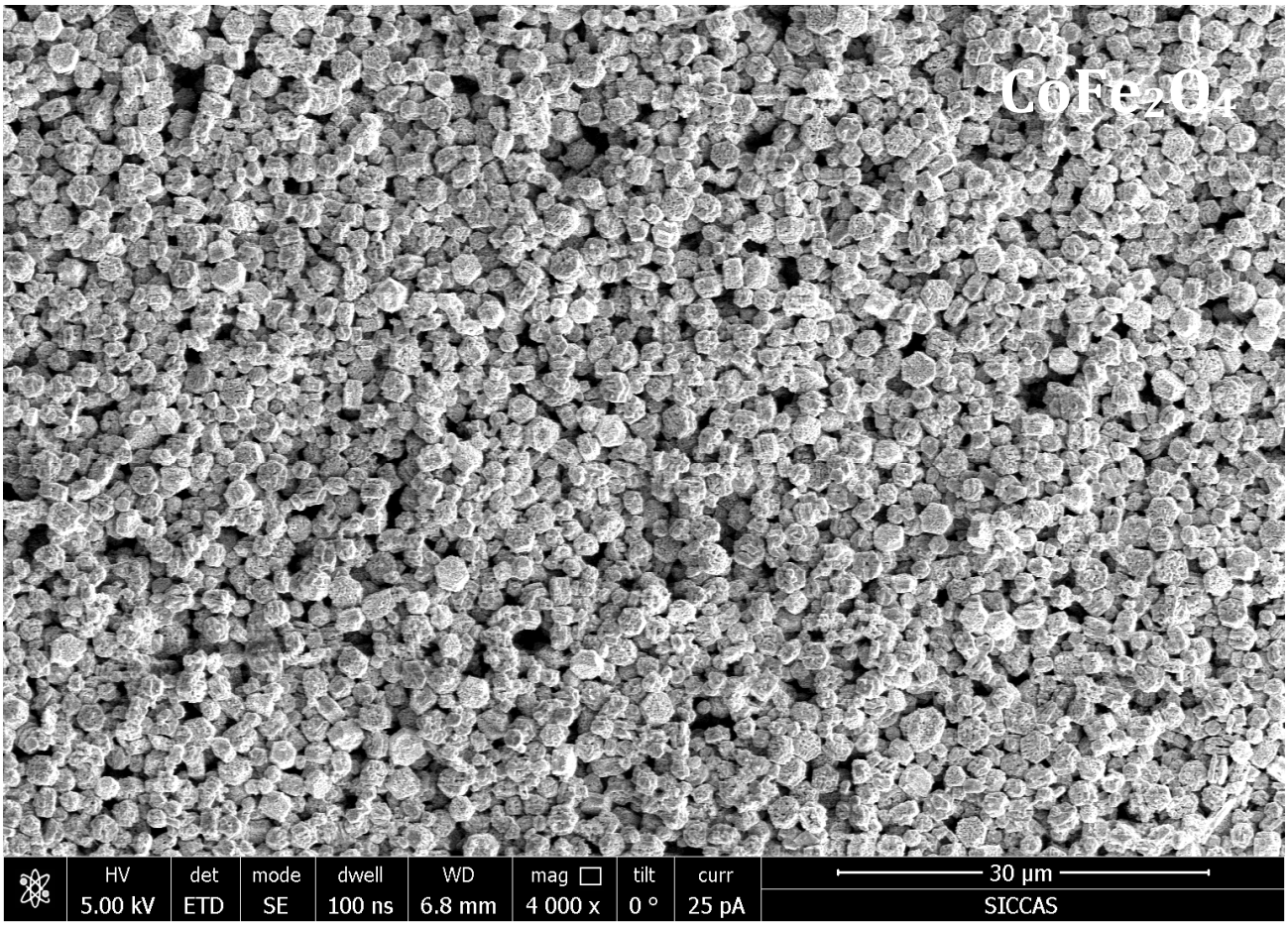

Figure 3b

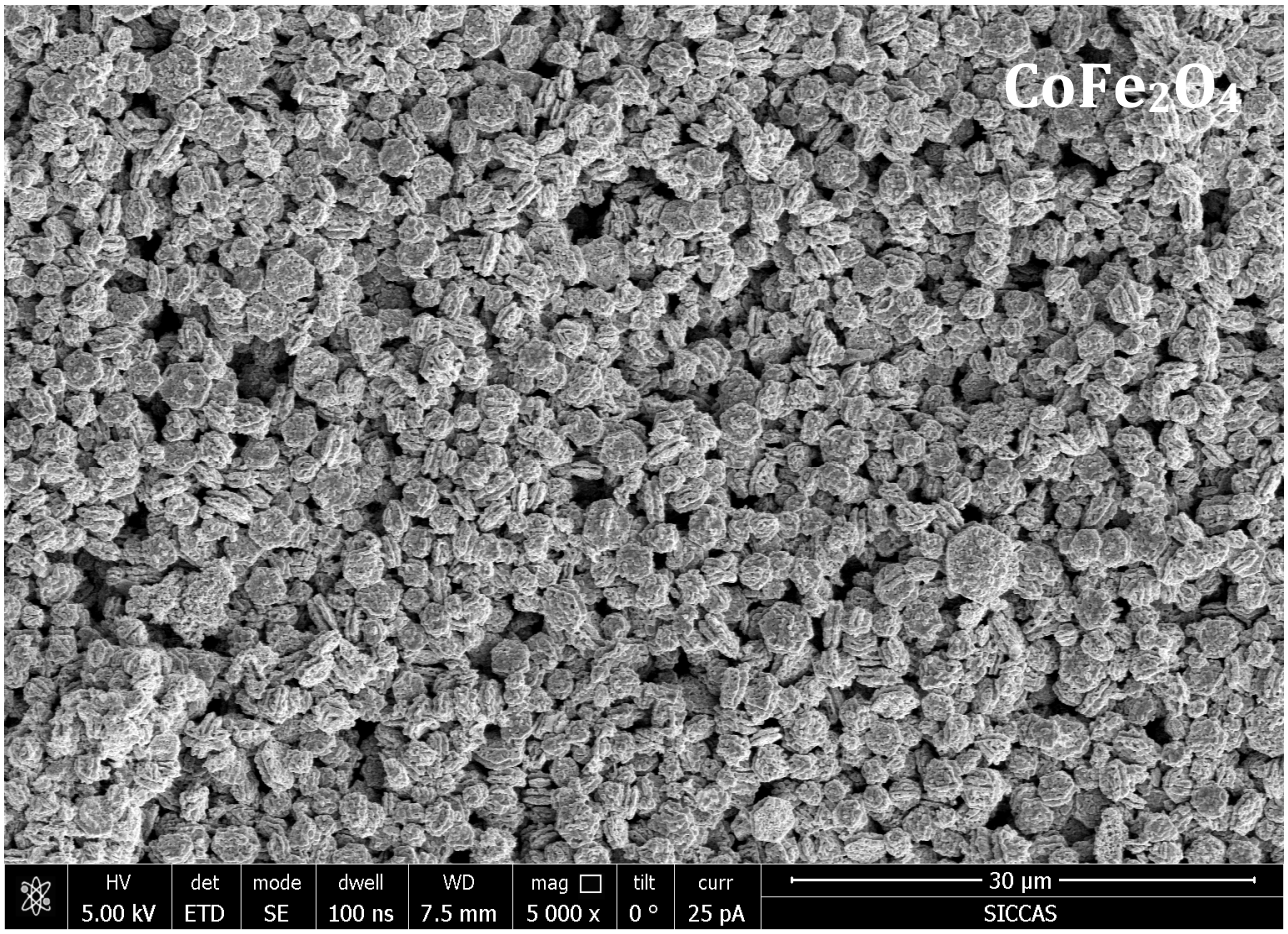

Figure 3c

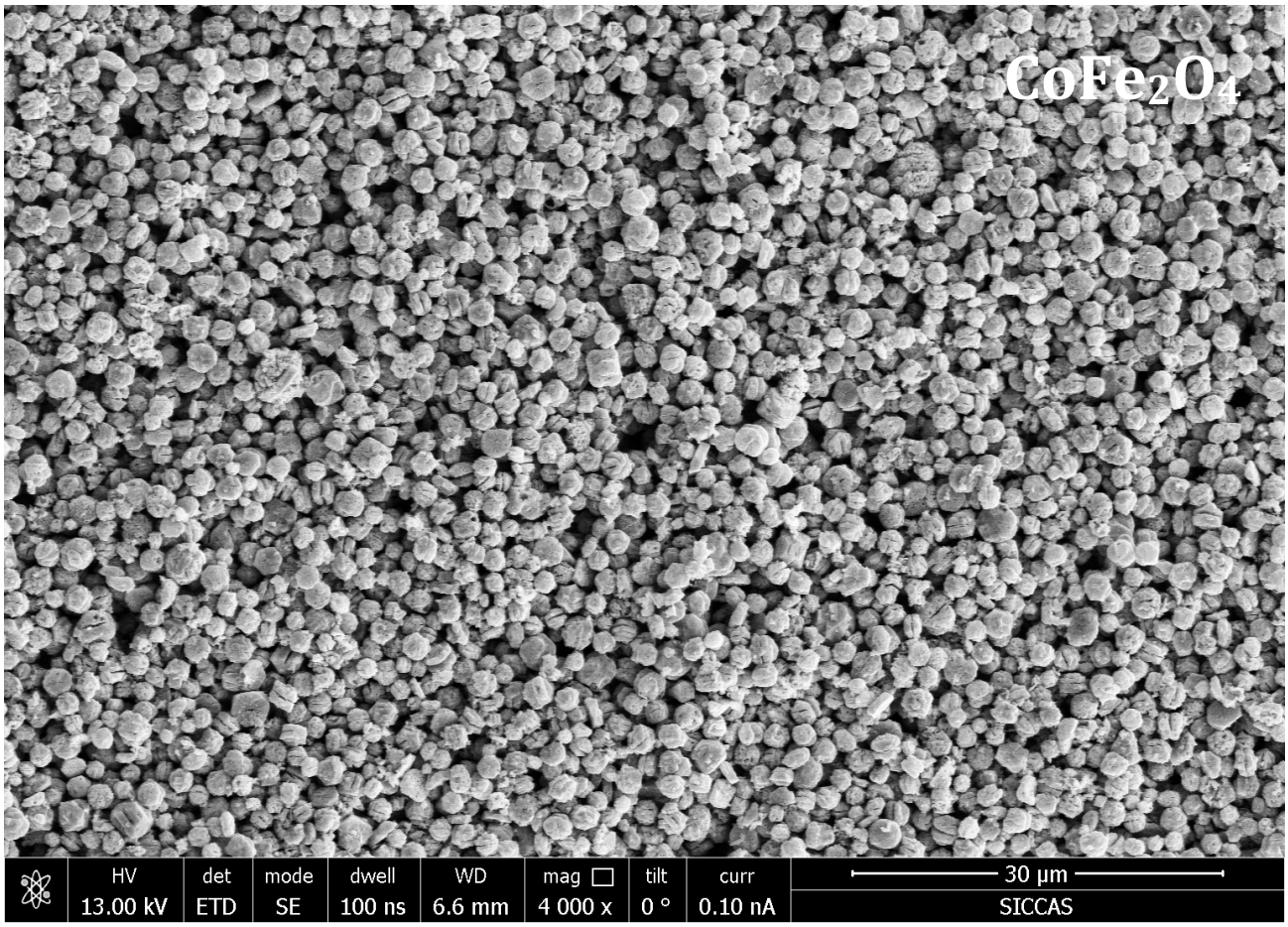

Figure 3e

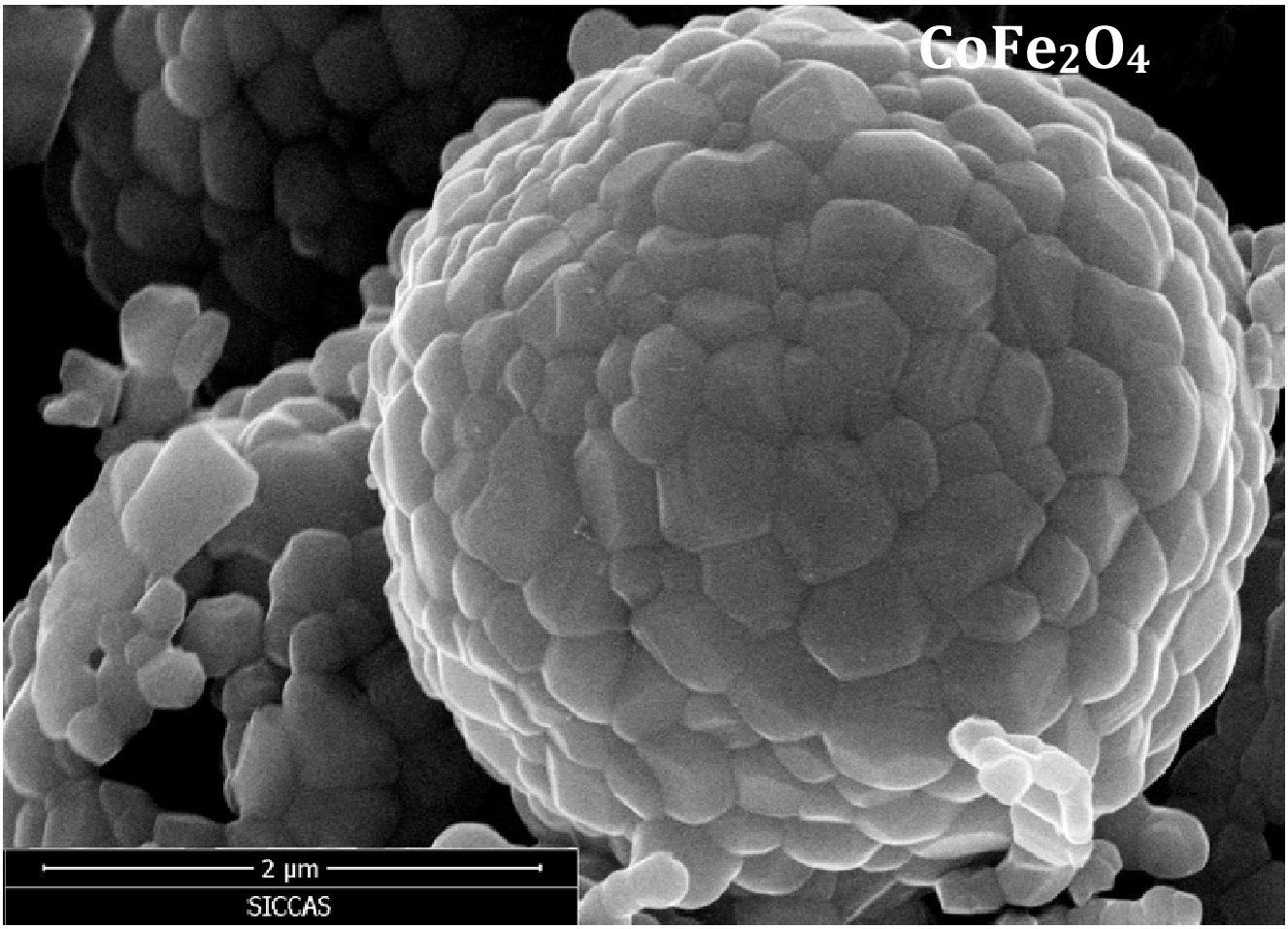

Figure 3e

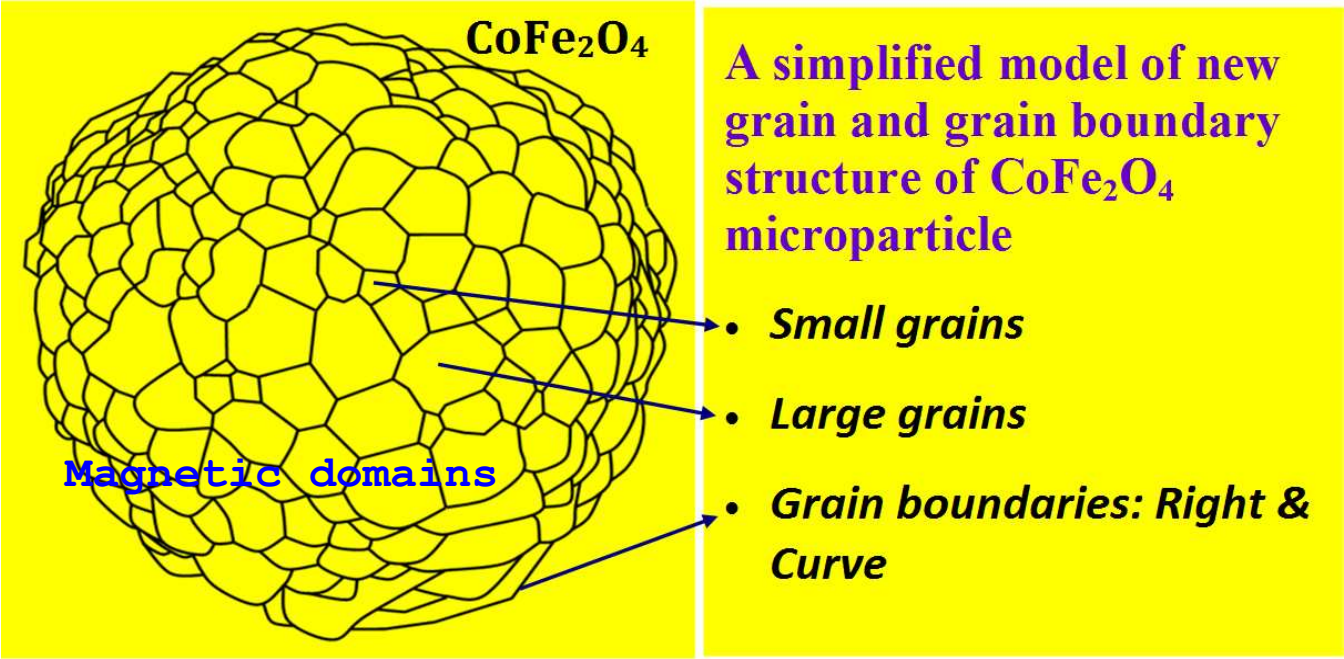

Figure 4

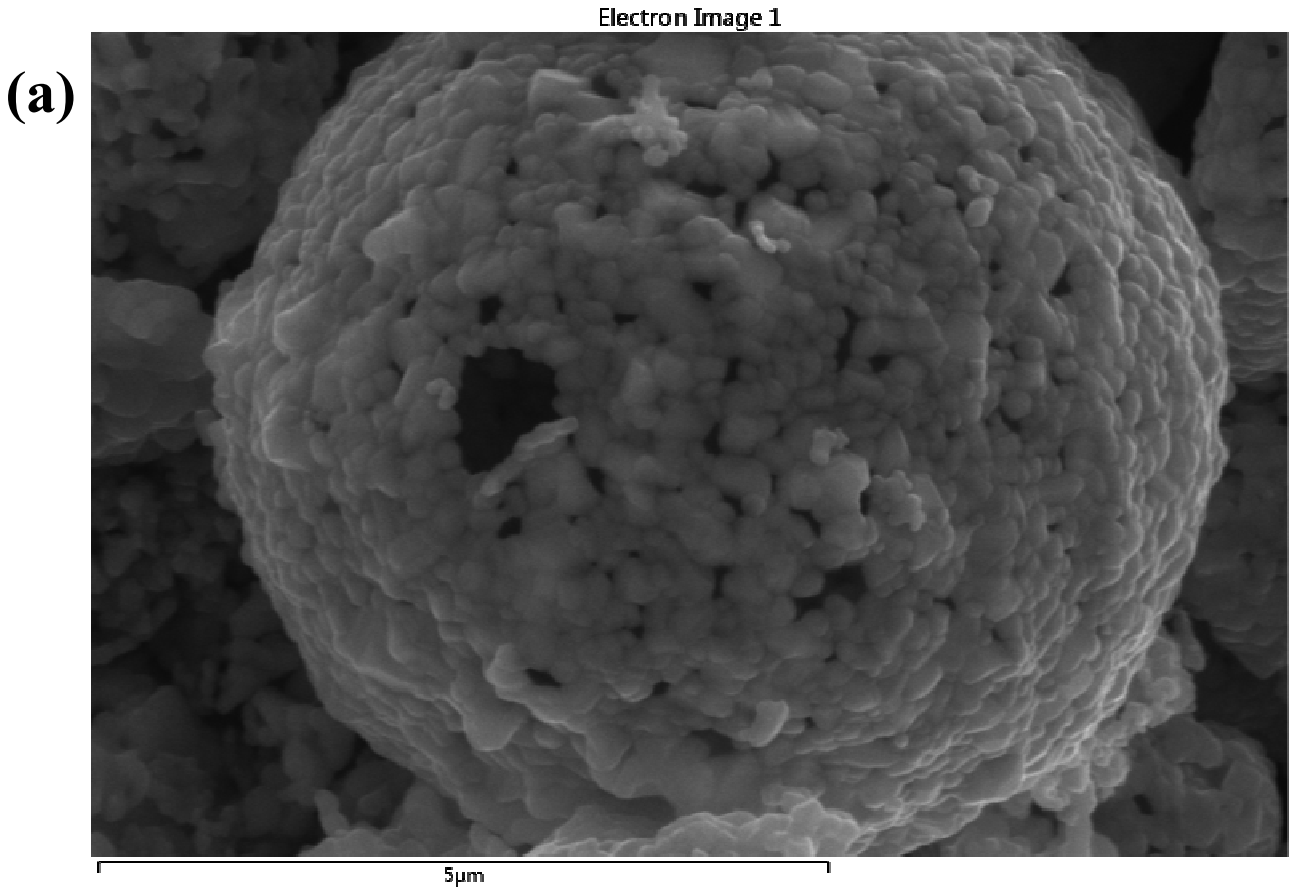

Figure 5

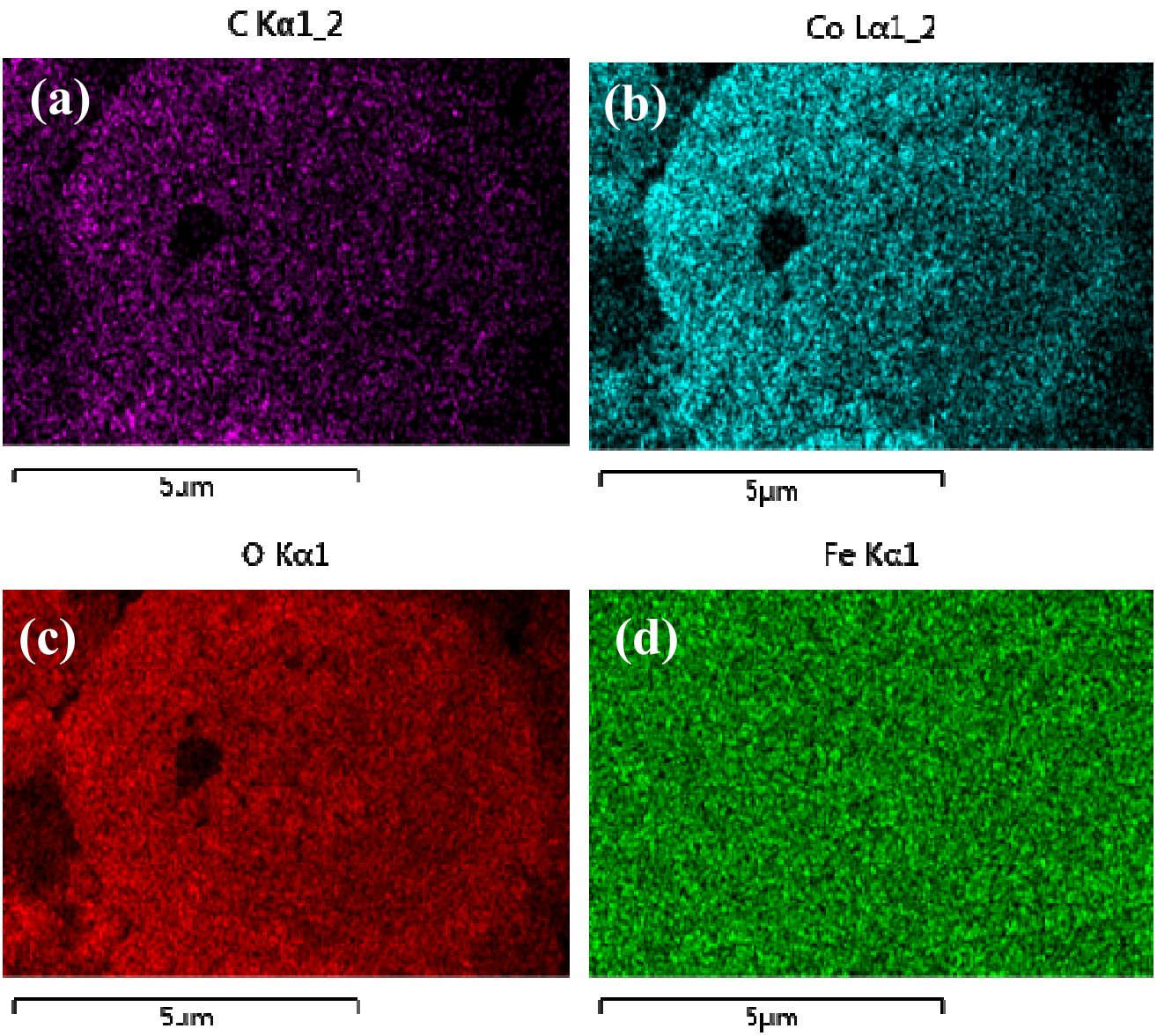

Figure 6

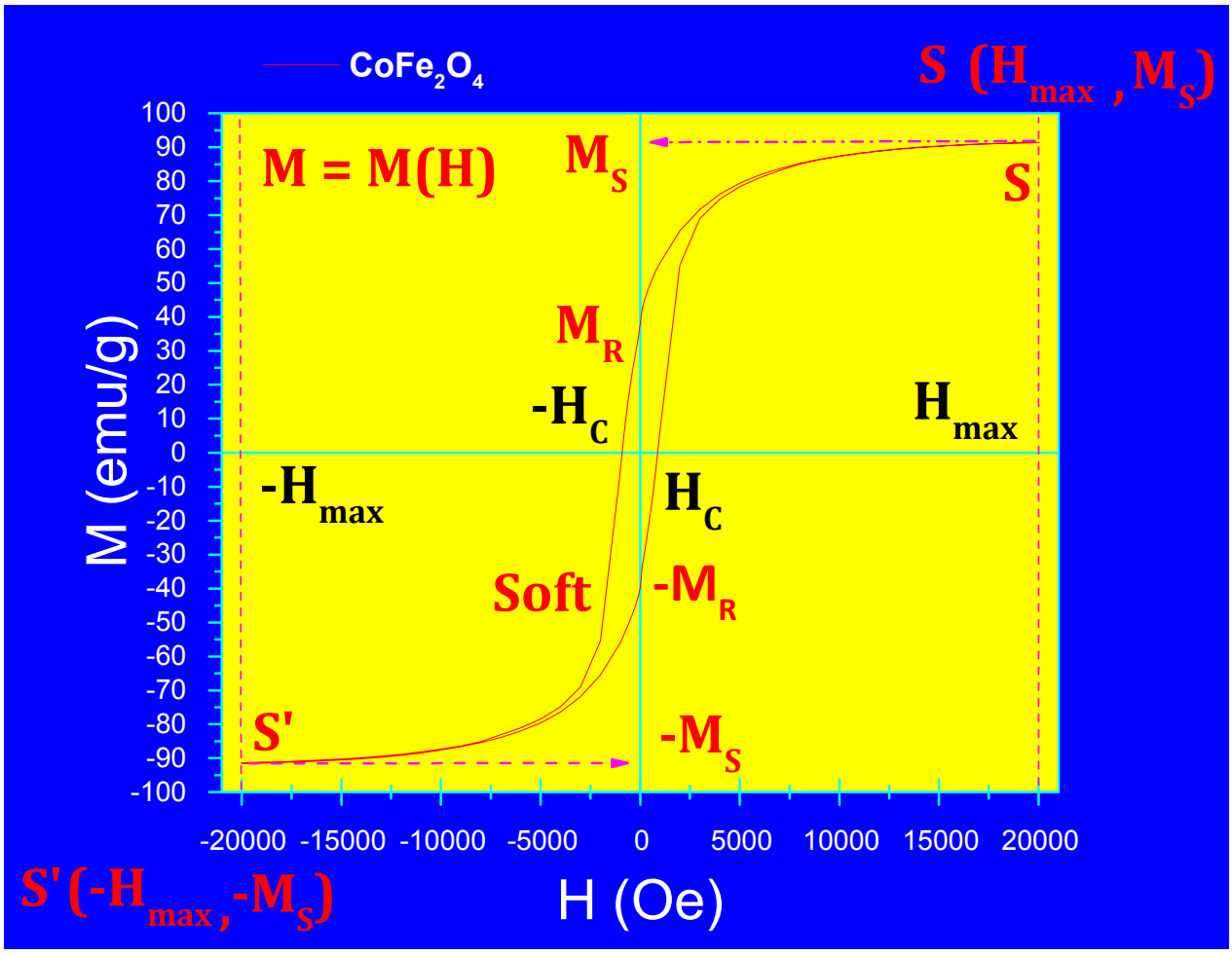

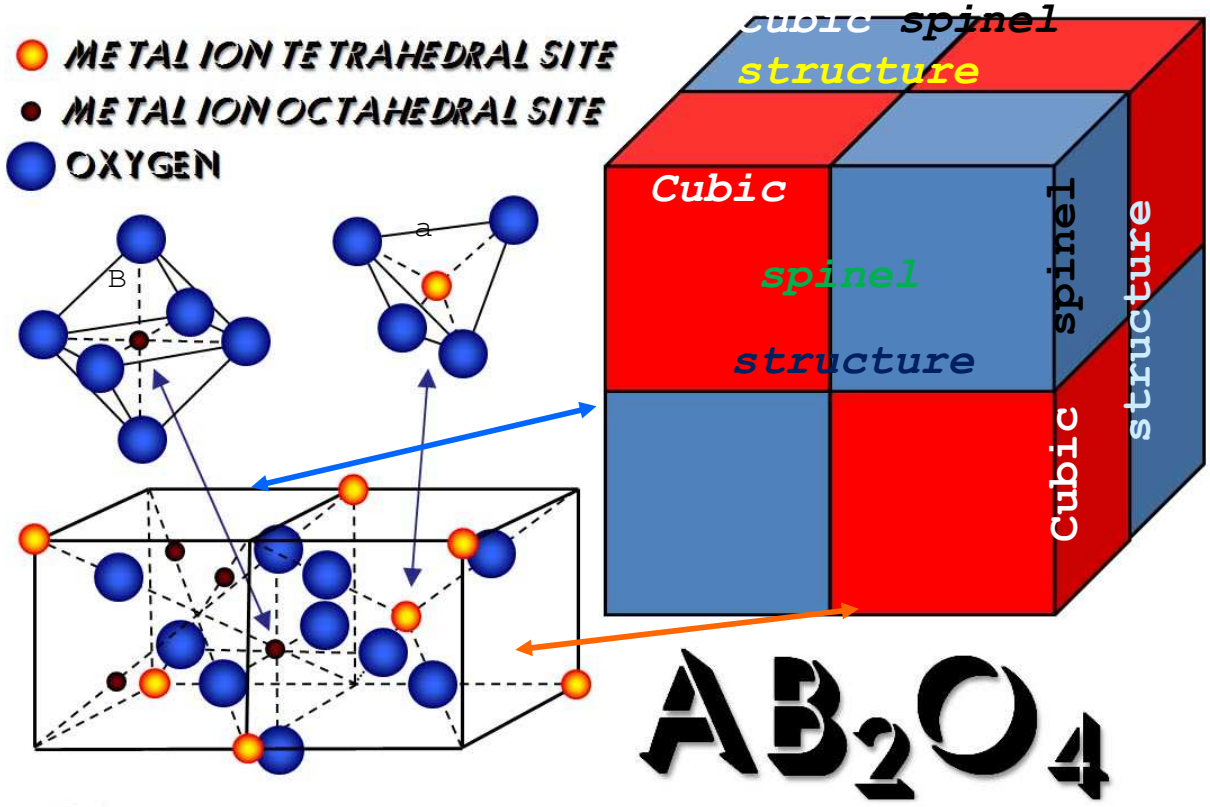

Figure 7a

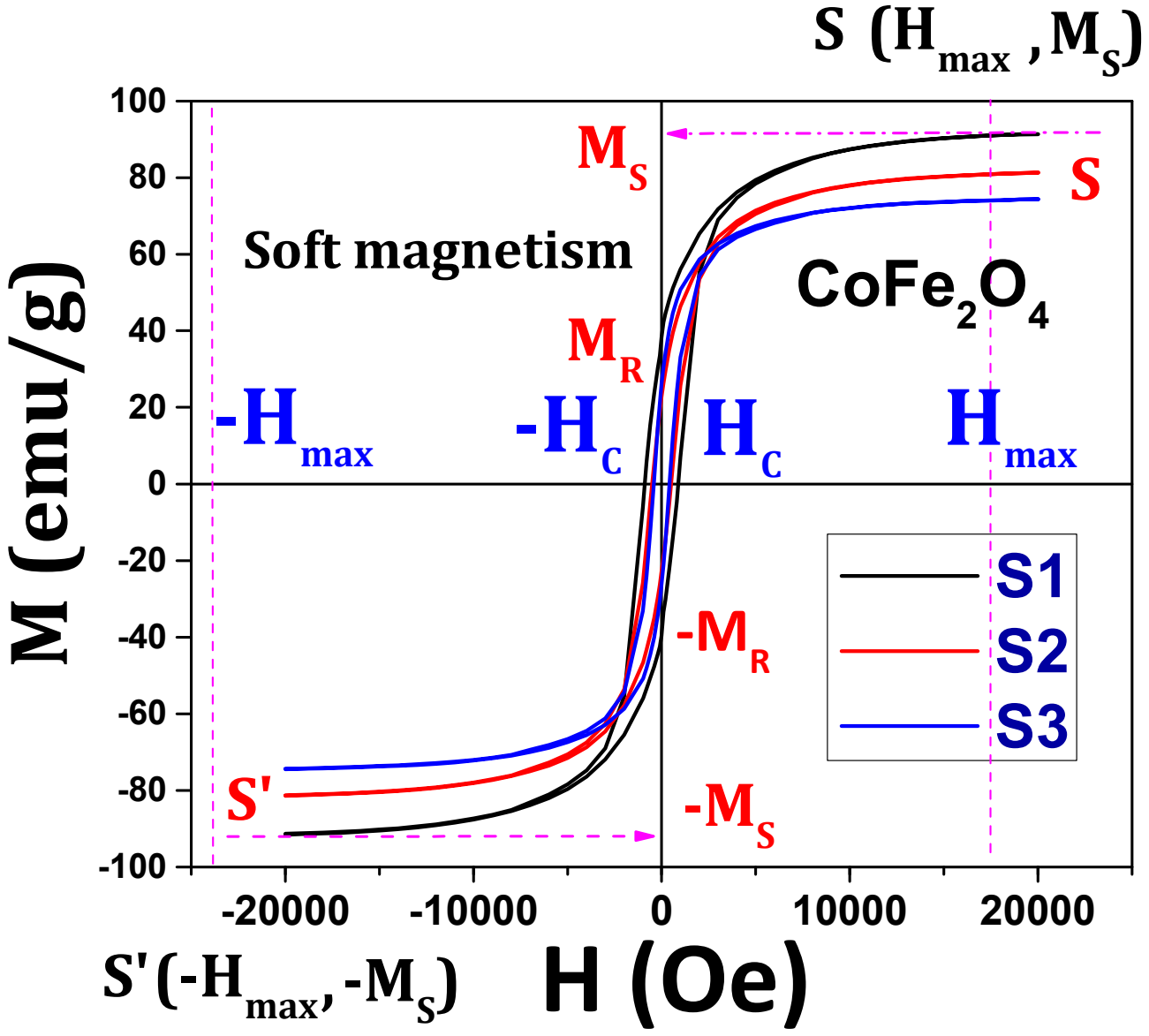

Figure 7b